Computers and Chemical Engineering 145 (2021) 107159

Contents lists available at ScienceDirect

Computers and Chemical Engineering

journal homepage: www.elsevier.com/locate/compchemeng

Model predictive control of a non-isothermal axial dispersion tubular reactor with recycle

Seyedhamidreza Khatibi, Guilherme Ozorio Cassol, Stevan Dubljevic*

Department of Chemical and Materials Engineering, University of Alberta, Edmonton, Alberta T6G 2V4, Canada

ARTICLE INFO

Article history:
Received 16 August 2020
Revised 11 October 2020
Accepted 3 November 2020
Available online 6 November 2020

Keywords:
Tubular reactor
Recycle systems
Model predictive control
Discrete observer
Coupled PDEs system

ABSTRACT

This paper addresses the model predictive output controller design for a non-isothermal axial dispersion tubular reactor accounting for energy and mass transport in a recycle stream. The underlying transport-reaction process is characterized by different mass and energy Peclet numbers. Open-loop analysis reveals unstable operating conditions based on the reactor's parameters. The discrete model of the system is obtained by considering a Crank-Nicolson type of discretization method without any model reduction and/or spatial approximation for the system of coupled parabolic PDEs. The proposed predictive controller accounts for asymptotic close-loop system stabilization and/or naturally present input and state constraints with the rejection of possible disturbances arising from reactor operations. To account for the output controller design, a discrete observer is developed to reconstruct the infinite dimensional states in the predictive control realization. Finally, the controller's performance is assessed via simulation studies, implying proper state stabilization and constraints satisfaction with input disturbance rejection.

© 2020 Elsevier Ltd. All rights reserved.

1. Introduction

Many transport-reaction processes present in petrochemical, biochemical and pharmaceutical unit operations belong to distributed parameter system (DPS) models. Within a finite spatial domain, the mathematical formulation of the mentioned processes, arising from the first-principle modeling, usually takes the form of a set of parabolic partial differential equations (PDEs) in which the intrinsic feature of reaction, convection and diffusion phenomena can be captured. The non-isothermal axial dispersion reactors have attracted great attention since their models account for a large number of reactor realizations in industry (see Varma and Aris, 1977 for a survey). In particular, the dynamical properties and control of axial dispersion tubular reactors, where mass and thermal phenomena are taking place, has been the objective of numerous studies over the years (see Hlavacek and Hofmann, 1970a; Hlavacek and Hofmann, 1970b; Cohen and Poore, 1974; Georgakis et al., 1977; Bokovi and Krsti, 2002), as several complexities are observed in the dynamic description and in the practical realization of the reactor operation (Marwaha and Luss, 2003). In addition, when a dispersive chemical tubular reactor is considered with a recycle of energy and mass flow, the model analysis and subsequent controller design become more challenging and require careful consideration since competitive effects of mass and heat transfer are present in the recycle, which may induce instability in apparently stable reactor operations (Luss and Amundson, 1967).

The salient feature of the axial dispersion reactor model is the mathematical description given by parabolic partial differential equations (PDEs), which can admit a variety of boundary modeling realizations to account for the physically meaningful setting present in the industry. Among several modeling realizations, the Danckwerts' boundary conditions (Danckwerts, 1953) reflect the physically relevant inlet flux transport and zero flux conditions at the reactor outlet. In general, the reactor models are numerically solved by the application of standard (high-order) and reduced-order PDE to ordinary differential equation (ODE) including finite difference discretization schemes (Badillo-Hernandez et al., 2019), methods relying on dynamically moving the discretization mesh to minimize the discretization error (Liu and Jacobsen, 2004), or by applying a variety of spectral methods, such as proper orthogonal decomposition (POD), to study oscillatory reactors' regimes (Bizon et al., 2008). Along with the modeling efforts, the controller designs and associated spatial discretization techniques are proposed for PDEs to obtain sets of ordinary differential equations (ODEs), and then the reduced models (if possible) are utilized for the synthesis of finite dimensional controllers (see Balas, 1979; Ray, 1981; Curtain, 1982; Antoniades and Christofides, 2000). The significant drawback of this approach, notably when it comes to parabolic PDEs, is the order of the discretization used (in the case of finite difference methods applied to approximate the

* Corresponding author.
E-mail addresses: khatibi@ualberta.ca (S. Khatibi), Stevan.Dubljevic@ualberta.ca (S. Dubljevic).

https://doi.org/10.1016/j.compchemeng.2020.107159
0098-1354/© 2020 Elsevier Ltd. All rights reserved.

spatial derivatives) and/or number of modes that must be considered to reach the desired order of model approximation, which may lead to high dimensional controllers that are difficult to be implemented. Consequently, the regulator design for dissipative PDEs has been the objective of many studies over the years. Different design methodologies were considered, such as approximate inertial manifolds, dynamic optimization, robust control, and linear quadratic control in the frequency domain (e.g. Christofides and Daoutidis, 1997;Armaou and Christofides, 2002;Aksikas et al., 2017 to cite a few). In the same vein, there are several contributions focused on the stability and dynamical properties of the axial dispersion tubular reactors with multiple steady states (Jensen and Ray, 1982; Dochain, 2018; Bildea et al., 2004).

Although the stabilization of the system is investigated in the aforementioned studies, the issue of input and state constraints, which are naturally present in the process, is generally not considered for the transport-reaction systems with recycle streams. Hence, within the optimal framework, the model predictive control (MPC), or the so-called online receding horizon control, is introduced by control practitioners to compute the required manipulated variable that optimizes the open-loop performance objective subjected to constraints (Muske and Rawlings, 1993). A significant number of contributions have been focused on properties of MPC controllers for parabolic PDEs, including spatial discretization methods, constraints validation with system performance for a class of the Riesz spectral systems with separable spectrums, piecewise predictive feedback control, and data-based modeling using repeated online linearization (Dufour et al., 2003; Dubljevic et al., 2006; Bonis et al., 2012).

For the implementation of digital controllers, the discrete version of the overall system is mainly required for control realizations. Over the years, for the conversion of the models or controllers into a discrete time setting, classical methods such as explicit or implicit Euler and Runge-Kutta methods are usually taken into account. It is proven from linear system theory that by increasing the sampling period, the accuracy of the discretization can be degraded, which leads to the mapping of stable continuous system into an unstable discrete one (Aström and Wittenmark, 1990; Kazantzis and Kravaris, 1999). This issue becomes more prominent when it comes to distributed parameter systems, given that the infinite dimensional state-space control realization needs to be accounted for in the controller design. Motivated by the aforementioned issues, this work considers a robust and accurate transformation of a continuous linear infinite dimensional system to a discrete one by the application of the Cayley-Tustin time discretization technique (Crank-Nicolson midpoint integration rule), in which the system properties and intrinsic energy of the DPS model are preserved (i.e., Hamiltonian preserving) (V. Havu and Malinen, 2007; Xu and Dubljevic, 2017). In addition, the practical realizations usually account for the output controller designs (Xie et al., 2019) due to the fact that infinite dimensional system states cannot be directly measured. Hence, the discrete observer developed in this work is based on the Cayley-Tustin method, which does not account for any model reduction or/and spatial approximation, as the discretization of the underlying operators is the usual procedure found in the literature to reconstruct the state variables given by transport-reaction processes (e.g. Dochain, 2001; Dochain, 2000; Mohd Ali et al., 2015; Alonso et al., 2004; Bitzer and Zeitz, 2002).

In this manuscript, the claimed novelty is the extension of linear MPC designs for the finite-dimensional system (Mayne, 2014; Rawlings et al., 2017) to the the infinite-dimensional one. Particularly, the transport-reaction system described by a system of coupled parabolic PDEs is considered, which might represent a non-isothermal axial dispersion tubular reactor with mass and thermal recycle flow. In addition, the proposed findings provide an insight into the dynamical properties of the system since the model of interest considers different mass and heat Peclet numbers in the spatial operators, accounting for the distinction between heat and mass transport phenomena. Moreover, different values of mass and thermal Peclet numbers lead to increased complexity in the model's representation and make it difficult to find the analytic solution for the eigenvalues and corresponding eigenfunctions. Due to the fact that one cannot realize the measurement of mass and temperature along the reactor, a discrete observer for the system of parabolic PDEs is proposed. The discrete-time observer design accounts for the available output measurement taken at the exit of the reactor (considered to be the reactor temperature) and reconstructs the system's states. Finally, the controller design provides optimal stabilization of the system with the inclusion of state and input constraints, as well as input disturbance rejection in the control law.

The manuscript is organized as follows: Section 2 addresses the model description of the axial dispersion tubular reactor with recycle. In Section 3, the linearized system is derived and the system is defined in an appropriate abstract Hilbert space. This is followed, in Section 4, by the linear system stability analysis and obtaining the relevant eigenfunctions and adjoint eigenfunctions of the system. In Section 5, the time discretization of the overall system is accomplished by the Cayley-Tustin technique. Then, the discrete observer design is provided in Section 6, while the optimization problem for coupled unstable parabolic PDEs is presented in Section 7. Finally, the performance of the proposed controller is demonstrated with a simulation study in Section 8.

2. Model formulation of an axial dispersion tubular reactor with recycle

2.1. Model representation

The chemical process shown in Fig. 1 represents a non-isothermal tubular reactor involving convection, molecular diffusion with macroscopic back mixing (dispersion) (Levenspiel, 1999), and a first-order irreversible reaction $A \rightarrow B$, where the reaction is considered to be exothermic. After passing through a separator, the unreacted component A is recycled and fed back to the tubular reactor. The dynamics of the system can be directly deduced from energy and mass balances on a slice with infinitesimal thickness dz shown in Fig. 1. The mentioned process is described by the class of convection-diffusion-reaction parabolic PDEs on domain $\{t_m \in \mathbb{R}^+, z \in [0, l_r]\}$ as follows (Jensen and Ray, 1982):

$$\begin{aligned}\frac{\partial C_A}{\partial t_m} &= D\frac{\partial^2 C_A}{\partial z^2} - v\frac{\partial C_A}{\partial z} - ke^{-\frac{E}{RT}}C_A \\ \frac{\partial T}{\partial t_m} &= \frac{\lambda}{\rho_f c_p}\frac{\partial^2 T}{\partial z^2} - v\frac{\partial T}{\partial z} - \frac{\Delta H_r}{\rho_f c_p}ke^{-\frac{E}{RT}}C_A + \frac{4h}{\rho C_p d_t}(T_c - T)\end{aligned} \tag{1}$$

assuming transport lags in the connecting lines are not significant, the associated Danckwerts boundary conditions (Danckwerts, 1953) are given by:

$$\begin{aligned}\left.\frac{\partial C_A}{\partial z}\right|_{z=0} &= \frac{v}{D}\left(C_A\Big|_{z=0} - (1-r)C_{A_{Feed}} - rC_A\Big|_{z=l_r}\right) \\ \left.\frac{\partial T}{\partial z}\right|_{z=0} &= \frac{\rho_f v c_p}{\lambda}\left(T\Big|_{z=0} - (1-r)T_{Feed} - rT\Big|_{z=l_r}\right) \\ \left.\frac{\partial C_A}{\partial z}\right|_{z=l_r} &= \left.\frac{\partial T}{\partial z}\right|_{z=l_r} = 0\end{aligned} \tag{2}$$

where the state components are $C_A(z, t_m)$ and $T(z, t_m)$ representing the concentration ($\frac{mol}{l}$) of reactant and the temperature (K) profile through the tubular reactor, respectively. $z \in [0, l_r]$ is the position

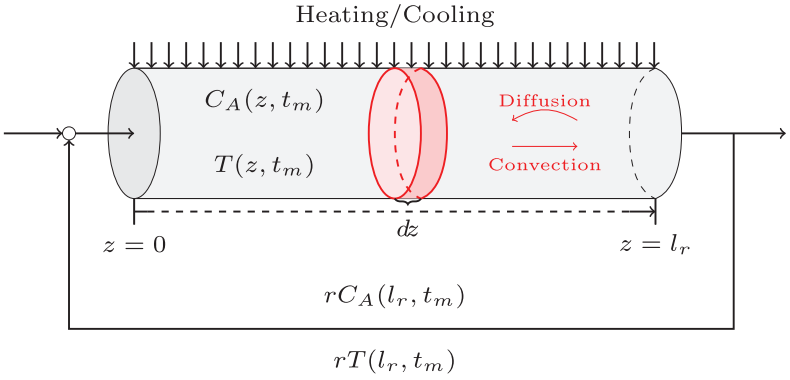

Fig. 1. Schematic view of the non-isothermal axial dispersion tubular reactor with recycle.

(m) and $t_m \geq 0$ is the time variable (s). The parameters of the axial dispersion reactor with recycle are given in Table A.1. For the sake of simplicity, one can transform the aforementioned system of equations into the dimensionless form by introducing the following change of coordinates:

$$\zeta = \frac{z}{l_r}, \ t = \frac{t_m v}{l_r} \tag{3}$$

As T_{Feed} and $C_{A_{Feed}}$ are considered to be constant values, the change of variables can be written as:

$$m_1 = \frac{C_{Feed} - C_A}{C_{Feed}}, \ m_2 = \frac{T - T_{Feed}}{T_{Feed}}, \ T_w(t) = \frac{T_c(t) - T_{Feed}}{T_{feed}} \tag{4}$$

By substitution, we get the following:

$$\begin{aligned}
&\frac{\partial m_1}{\partial t} = \frac{1}{Pe_m}\frac{\partial^2 m_1}{\partial \zeta^2} - \frac{\partial m_1}{\partial \zeta} + k_a(1-m_1)e^{\left(\frac{\eta m_2}{1+m_2}\right)} \\
&\frac{\partial m_2}{\partial t} = \frac{1}{Pe_T}\frac{\partial^2 m_2}{\partial \zeta^2} - \frac{\partial m_2}{\partial \zeta} + \delta k_a(1-m_1)e^{\left(\frac{\eta m_2}{1+m_2}\right)} + \sigma(T_w - m_2) \\
&\frac{\partial m_1}{\partial \zeta}\Big|_{\zeta=0} = Pe_m\left(m_1\Big|_{\zeta=0} - r m_1\Big|_{\zeta=1}\right) \\
&\frac{\partial m_2}{\partial \zeta}\Big|_{\zeta=0} = Pe_T\left(m_2\Big|_{\zeta=0} - r m_2\Big|_{\zeta=1}\right) \\
&\frac{\partial m_1}{\partial \zeta}\Big|_{\zeta=1} = \frac{\partial m_2}{\partial \zeta}\Big|_{\zeta=1} = 0
\end{aligned} \tag{5}$$

with:

$$Pe_m = \frac{v l_r}{D}, Pe_T = \frac{\rho v C_p l_r}{\lambda}, k_a = \frac{k l_r}{v} e^{-\eta},$$

$$\delta = \frac{-\Delta H_r C_{A_{Feed}}}{\rho C_p T_{Feed}}, \eta = \frac{E}{R T_{Feed}}, \sigma = \frac{4 h l_r}{\rho C_p v d_t}$$

Pe_m and Pe_T are defined as mass and heat Peclet numbers, respectively. The dimensionless Peclet numbers describe the relative significance of diffusion and convection in the chemical tubular reactor shown in Fig. 1.

2.2. Steady state solutions

The steady state solutions of the reaction-convection-diffusion PDEs in Eq. (5) can be obtained by solving the following ordinary differential equations with their associated boundary conditions:

$$\begin{aligned}
&\frac{1}{Pe_m}\frac{d^2 m_{1_{ss}}}{d\zeta^2} - \frac{d m_{1_{ss}}}{d\zeta} + k_a(1-m_{1_{ss}})e^{\left(\frac{\eta m_{2_{ss}}}{1+m_{2_{ss}}}\right)} = 0 \\
&\frac{1}{Pe_T}\frac{d^2 m_{2_{ss}}}{d\zeta^2} - \frac{d m_{2_{ss}}}{d\zeta} + \delta k_a(1-m_{1_{ss}})e^{\left(\frac{\eta m_{2_{ss}}}{1+m_{2_{ss}}}\right)} + \sigma(T_{w_{ss}} - m_{2_{ss}}) = 0 \\
&\frac{d m_{1_{ss}}}{d\zeta}\Big|_{\zeta=0} = Pe_m\left(m_{1_{ss}}\Big|_{\zeta=0} - r m_{1_{ss}}\Big|_{\zeta=1}\right) \\
&\frac{d m_{2_{ss}}}{d\zeta}\Big|_{\zeta=0} = Pe_T\left(m_{2_{ss}}\Big|_{\zeta=0} - r m_{2_{ss}}\Big|_{\zeta=1}\right) \\
&\frac{d m_{1_{ss}}}{d\zeta}\Big|_{\zeta=1} = \frac{d m_{2_{ss}}}{d\zeta}\Big|_{\zeta=1} = 0
\end{aligned} \tag{6}$$

It is well-known in the literature that due to the nonlinearity in the kinetic term, representing the interconnection of temperature and concentration, particularly for exothermic reactions, multiple steady state profiles, either stable or unstable, can be generated (Heinemann and Poore, 1982; Hastir et al., 2020). It is important to point out that in practical applications, the operating points of interest may correspond to an unstable equilibrium profile observed by the above equations.

By considering the following parameters and using the shooting method, one can identify the existence of multiple equilibrium profiles as it is illustrated in Fig. 2:

$$Pe_m = 4, \ Pe_T = 6, \ T_{feed} = 600, \ T_{w_{ss}} = 380, \ C_{A_{feed}} = 1,$$

$$\sigma = 0.9, \ k_a = 0.6, \ \delta = 0.8, \ \eta = 20$$

The results show that three steady state solutions are possible solutions to the system given by Eq. (6). In order to study the impact of the recycle ratio on multiplicity analysis, the aforementioned parameters have been used with different recycle ratios. Since the amount of fresh feed decreases as the recycle ratio increases, one can realize the generated reactor hot spot decreases, see Fig. 2. Moreover, it can be understood as the recycle ratio increases, the temperature of stable equilibria (dashed line) drops until it converges into the unstable equilibrium profile. The equilibrium profile of interest is the middle one between the low and high conversion profiles (represented by dash-dotted lines). As expected, this is the unstable equilibrium profile obtained by Eq. (6). Therefore, it is important to implement a robust and reliable controller to keep the tubular reactor working at unstable operating points. In the following sections, the stability analysis is performed and, subsequently, the design of the model predictive controller is addressed based on the linearized model around the unstable equilibrium profile.

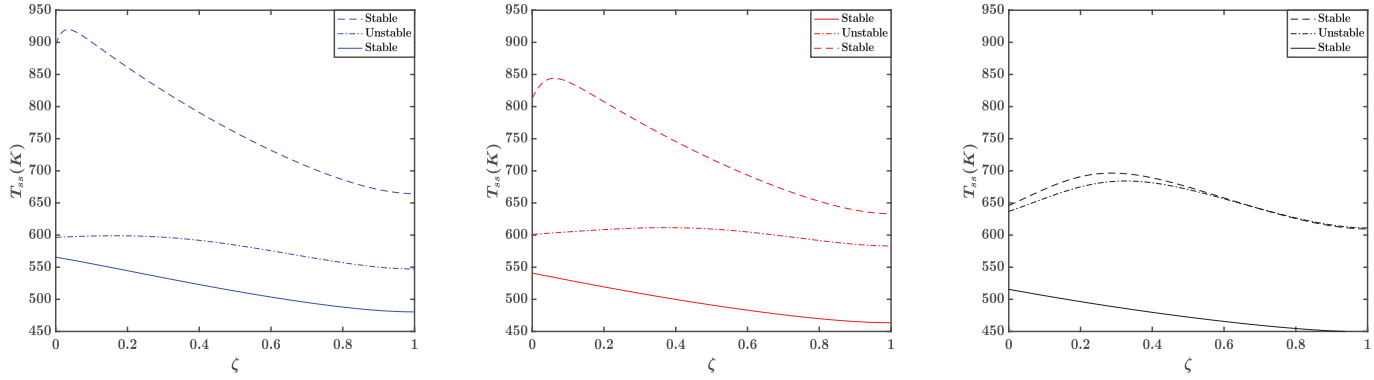

(a) $r = 0.15$ (b) $r = 0.3$ (c) $r = 0.45$

Fig. 2. Comparison of the multiple steady state profiles with different values for recycle ratio.

3. Linearized model

3.1. System linearization

Consider the following deviation variables:

$$\begin{bmatrix} x_1(\zeta,t) = m_1(\zeta,t) - m_{1_{ss}}(\zeta) \\ x_2(\zeta,t) = m_2(\zeta,t) - m_{2_{ss}}(\zeta) \end{bmatrix} \tag{7}$$

we assume the cooling jacket temperature ($T_c(t)$) as the manipulated input variable and the reactor outlet temperature as the measured output of the system, which is required to reconstruct the states in the subsequent observer design. Then, the new input and output can be defined as follows:

$$\begin{bmatrix} u(t) = T_w(t) - T_{w_{ss}} \\ y(t) = m_2(\zeta = 1,t) - m_{2_{ss}}(\zeta = 1) \end{bmatrix} \tag{8}$$

The reaction rate is linearized around its steady-state as it depends on the dimensionless concentration and temperature of the reactor:

$$\begin{aligned} &f_{nl}(m_1,m_2) = k_a(1-m_1)e^{\frac{\eta m_2}{1+m_2}} \approx f_{nl}(m_{1_{ss}},m_{2_{ss}}) + \\ &R_1(m_1 - m_{1_{ss}}) + R_2(m_2 - m_{2_{ss}}), \\ &g_{nl}(m_1,m_2) = \delta k_a(1-m_1)e^{\frac{\eta m_2}{1+m_2}} \approx \delta g_{nl}(m_{1_{ss}},m_{2_{ss}}) \\ &+\delta R_1(m_1 - m_{1_{ss}}) + \delta R_2(m_2 - m_{2_{ss}}) \end{aligned} \tag{9}$$

with the following coefficients:

$$R_1(\zeta) = -k_a e^{\frac{\eta m_{2_{ss}}(\zeta)}{1+m_{2_{ss}}(\zeta)}},\ R_2(\zeta) = \frac{\eta k_a(1-m_{1_{ss}}(\zeta))e^{\frac{\eta m_{2_{ss}}(\zeta)}{1+m_{2_{ss}}(\zeta)}}}{(1+m_{2_{ss}}(\zeta))^2}$$

where $R_1(\zeta)$, $R_2(\zeta)$, $\delta R_1(\zeta)$ and $\delta R_2(\zeta)$ are the elements of the Jacobian matrix. In the linearized system, we consider the spatial averaged coefficients over the space ($\bar{R}_1$ and $\bar{R}_2$), defined as below:

$$\begin{cases} \bar{R}_1 = \int_0^1 R_1(\zeta)d\zeta \\ \bar{R}_2 = \int_0^1 R_2(\zeta)d\zeta \end{cases} \tag{10}$$

Finally, the linearized representation of the original system in Eq. (5) takes the following form:

$$\begin{aligned} &\frac{\partial x_1}{\partial t} = \frac{1}{Pe_m}\frac{\partial^2 x_1}{\partial \zeta^2} - \frac{\partial x_1}{\partial \zeta} + \bar{R}_1 x_1 + \bar{R}_2 x_2 \\ &\frac{\partial x_2}{\partial t} = \frac{1}{Pe_T}\frac{\partial^2 x_2}{\partial \zeta^2} - \frac{\partial x_2}{\partial \zeta} + \delta\bar{R}_1 x_1 + \delta\bar{R}_2 x_2 + \sigma(u(t) - x_2) \\ &\frac{\partial x_1}{\partial \zeta}\Big|_{\zeta=0} = Pe_m\left(x_1\Big|_{\zeta=0} - r x_1\Big|_{\zeta=1}\right) \\ &\frac{\partial x_2}{\partial \zeta}\Big|_{\zeta=0} = Pe_T\left(x_2\Big|_{\zeta=0} - r x_2\Big|_{\zeta=1}\right) \\ &\frac{\partial x_1}{\partial \zeta}\Big|_{\zeta=1} = \frac{\partial x_2}{\partial \zeta}\Big|_{\zeta=1} = 0, \\ &y(t) = x_2\Big|_{\zeta=1} \end{aligned} \tag{11}$$

3.2. Infinite-dimensional system representation

The system of coupled parabolic PDEs given by Eq. (11) can be rewritten as the following state space equations:

$$\begin{aligned} &\dot{x}(\zeta,t) = Ax(\zeta,t) + Bu(t) \\ &y(t) = Cx(\zeta,t) \end{aligned} \tag{12}$$

where x is the state, $x(\zeta,t) = \begin{bmatrix} x_1(\zeta,t) \\ x_2(\zeta,t) \end{bmatrix}$, and the operator A is defined as a linear operator $\mathfrak{L}(X)$ (X is defined as Hilbert space $L^2[0,1] \times L^2[0,1]$):

$$\begin{aligned} A(\cdot) &= \begin{bmatrix} \frac{1}{Pe_m}\frac{\partial^2}{\partial\zeta^2} - \frac{\partial}{\partial\zeta} + \bar{R}_1 & \bar{R}_2 \\ \delta\bar{R}_1 & \frac{1}{Pe_T}\frac{\partial^2}{\partial\zeta^2} - \frac{\partial}{\partial\zeta} + \delta\bar{R}_2 - \sigma \end{bmatrix}(\cdot) \\ &= \begin{bmatrix} A_{11} & A_{12} \\ A_{21} & A_{22} \end{bmatrix}(\cdot) \end{aligned} \tag{13}$$

such that $D(A) = \Big\{ x = (x_1,x_2)^T \in X : x(\zeta) \in L^2[0,1] \Big| x(\zeta),\ \frac{dx}{d\zeta},\ \frac{d^2x}{d\zeta^2}$ a.c., $\frac{dx_1}{d\zeta}\Big|_{\zeta=1} = \frac{dx_2}{d\zeta}\Big|_{\zeta=1} = 0$, $\frac{dx_1}{d\zeta}\Big|_{\zeta=0} = Pe_m\left(x_1\Big|_{\zeta=0} - r x_1\Big|_{\zeta=1}\right)$ and $\frac{dx_2}{d\zeta}\Big|_{\zeta=0} = Pe_T\left(x_2\Big|_{\zeta=0} - r x_2\Big|_{\zeta=1}\right) \Big\}$. Moreover, the actuation $B = \begin{bmatrix} 0 \\ \sigma \end{bmatrix}$ represents the linear input operator $\mathfrak{L}(\mathbb{R},X)$, and $C = \begin{bmatrix} 0 & \int_0^1 \delta(\zeta-1)(.)d\zeta \end{bmatrix}$ indicates the linear output operator providing boundary point observation in the control setting. The spatial differential operator A has a well-defined eigenvalue problem, which depends on the Peclet numbers and recycle ratio r. The solution of the eigenvalue problem provides spectral system characteristics, such as eigenvalues and associated eigenfunctions.

4. Linear system stability analysis ($Pe_T \neq Pe_m$)

Based on the linear system representation, it is possible to analyze the internal stability by solving the eigenvalue problem associated with the system, see Eq. (11). In particular, the stability assessment is performed with different settings of the Peclet numbers, which is studied less often in the literature (see Hastir et al., 2020), as the constant value for Peclet numbers ($Pe_T = Pe_m$) implies the assumption of same transport properties of the mass and heat flow in the axial dispersion reactor, see Antoniades and Christofides (2000, 2001) as examples of this case.

Consequently, the eigenvalues (λ) and eigenfunctions of the operators A and A^* will be specified to access the system stability and to determine the terminal cost in the model predictive controller, which will be demonstrated in the following sections.

4.1. Eigenvalues and eigenfunctions of the operator A

The linear system representation is utilized to analyze the internal stability of the operator A by solving the following eigenvalue problem for the unforced ($u(t) = 0$) coupled parabolic PDEs:

$$A\Phi = \lambda\Phi \tag{14}$$

where the operator A is defined by Eq. (13). The associated vector of eigenfunctions $\Phi(\zeta)$ is constructed as follows:

$$\Phi(\zeta) = \begin{bmatrix} \Phi_1(\zeta) \\ \Phi_2(\zeta) \end{bmatrix} \tag{15}$$

by substitution in Eq. (14), one can get the system of second order ordinary differential equations. The system can be rewritten as $\dot{Y}(\zeta) = \bar{A}Y$, where $\bar{A}$ is a matrix with constant components and Y is defined as the vector of eigenfunctions (Φ_1, Φ_2) with their derivatives:

$$\bar{A} = \begin{bmatrix} 0 & 1 & 0 & 0 \\ Pe_m(\lambda - \bar{R}_1) & Pe_m & -Pe_m\bar{R}_2 & 0 \\ 0 & 0 & 0 & 1 \\ -Pe_T\delta\bar{R}_1 & 0 & Pe_T(\lambda + \sigma - \delta\bar{R}_2) & Pe_T \end{bmatrix}, \quad Y = \begin{bmatrix} \Phi_1 \\ \frac{d\Phi_1}{d\zeta} \\ \Phi_2 \\ \frac{d\Phi_2}{d\zeta} \end{bmatrix} \tag{16}$$

Hence, the solution can be expressed as:

$$Y(\zeta) = e^{\bar{A}(\zeta-1)}Y(1) = N_{i,j}Y(1) \tag{17}$$

$N_{4\times4}(\zeta)$ is defined as the exponential matrix, with index i and j referring to each element of the matrix. Applying the boundary conditions presented in Eq. (11) leads to the following nonlinear equation, which is numerically solvable and gives the system's eigenvalues:

$$f(\lambda) = k_1k_4 - k_2k_3 = 0 \tag{18}$$

with:

$$\begin{aligned} k_1 &= Pe_mN_{1,1}^{(\zeta=0)} - N_{2,1}^{(\zeta=0)} - Pe_mr, \\ k_2 &= Pe_mN_{1,3}^{(\zeta=0)} - N_{2,3}^{(\zeta=0)}, \\ k_3 &= Pe_mN_{3,1}^{(\zeta=0)} - N_{4,1}^{(\zeta=0)}, \\ k_4 &= Pe_TN_{3,3}^{(\zeta=0)} - N_{4,3}^{(\zeta=0)} - Pe_Tr \end{aligned} \tag{19}$$

Remark 1. In this work, as a system with different Peclet numbers and the Danckwerts' conditions is considered, finding the analytic solution for spectral system characteristics is not applicable. Thus, the numerical solution for this equation is presented.

The solution of Eq. (19) generates the eigenvalue spectrum containing the stable and unstable modes (λ_u, λ_s) associated with corresponding eigenfunctions (Φ_u, Φ_s) constructed as the function basis of the operator A in Eq. (13). Thus, based on Eq. (18), the eigenvalue problem is solved for the unstable equilibrium profile, see Fig. 2. In addition, from Fig. 3, it can be seen that there is only one real unstable eigenvalue generated by the coupled parabolic PDEs system with the operating conditions considered. It is interesting to explore the relative importance of the mass and heat Peclet numbers on the calculated eigenvalues of the system. Hence, by changing the values for the mass diffusivity and energy dispersion coefficient, which are related to Pe_m and Pe_T, new steady state solutions are found and, once again, the eigenvalue problem is solved for the unstable equilibrium profile. The eigenvalues' distributions are presented in Fig. 3. In this case, it is possible to see that increasing Pe_m and Pe_T leads to more complex eigenvalues. In Section 7.1, the stabilization of the system will be addressed by rejecting the unstable modes under the developed model predictive controller.

4.2. Eigenfunctions of the operator A*

For any $x \in D(A)$ and $y \in D(A^*)$, one can write the following definition:

$$< Ax, y > = < x, A^*y > \tag{20}$$

employing integration by parts and substituting the boundary conditions given in Eq. (11), results in the following adjoint operator A^* (see Appendix B):

$$\begin{aligned} A^*(\cdot) &= \begin{bmatrix} \frac{1}{Pe_m}\frac{\partial^2}{\partial\zeta^2} + \frac{\partial}{\partial\zeta} + \bar{R}_1 & \delta\bar{R}_1 \\ \bar{R}_2 & \frac{1}{Pe_T}\frac{\partial^2}{\partial\zeta^2} + \frac{\partial}{\partial\zeta} + \delta\bar{R}_2 - \sigma \end{bmatrix}(\cdot) \\ &= \begin{bmatrix} A_{11}^* & A_{12}^* \\ A_{21}^* & A_{22}^* \end{bmatrix}(\cdot) \end{aligned} \tag{21}$$

with the new boundary conditions represented as below:

$$\begin{aligned} \left.\frac{\partial y_1}{\partial\zeta}\right|_{\zeta=1} &= -Pe_m\left(y_1\Big|_{\zeta=1} - ry_1\Big|_{\zeta=0}\right) \\ \left.\frac{\partial y_2}{\partial\zeta}\right|_{\zeta=1} &= -Pe_T\left(y_2\Big|_{\zeta=1} - ry_2\Big|_{\zeta=0}\right) \\ \left.\frac{\partial y_1}{\partial\zeta}\right|_{\zeta=0} &= \left.\frac{\partial y_2}{\partial\zeta}\right|_{\zeta=0} = 0 \end{aligned} \tag{22}$$

A similar procedure, as described in Section 4.1, is followed to compute the adjoint eigenfunctions of the coupled parabolic PDEs system. The associated vector of adjoint eigenfunctions is given by:

$$\Phi^*(\zeta) = \begin{bmatrix} \Phi_1^*(\zeta) \\ \Phi_2^*(\zeta) \end{bmatrix} \tag{23}$$

Finally, we define $\hat{\Phi}_m(\zeta)$ and $\hat{\Phi}_n^*(\zeta)$ as the normalized eigenfunctions and corresponding bi-orthogonal ones, respectively. Indeed, based on Eqs. (15)–(23) they can be constructed by:

$$\begin{aligned} \hat{\Phi}_m(\zeta) &= \frac{\Phi_m(\zeta)}{\sqrt{\int_0^1 \left(\Phi_{1_m}(\zeta)\Phi_{1_m}^*(\zeta) + \Phi_{2_m}(\zeta)\Phi_{2_m}^*(\zeta)\right)d\zeta}} \\ \hat{\Phi}_n^*(\zeta) &= \frac{\Phi_n^*(\zeta)}{\sqrt{\int_0^1 \left(\Phi_{1_n}(\zeta)\Phi_{1_n}^*(\zeta) + \Phi_{2_n}(\zeta)\Phi_{2_n}^*(\zeta)\right)d\zeta}} \end{aligned} \tag{24}$$

where indices m, n indicate the corresponding eigenvalue of the coupled parabolic PDEs.

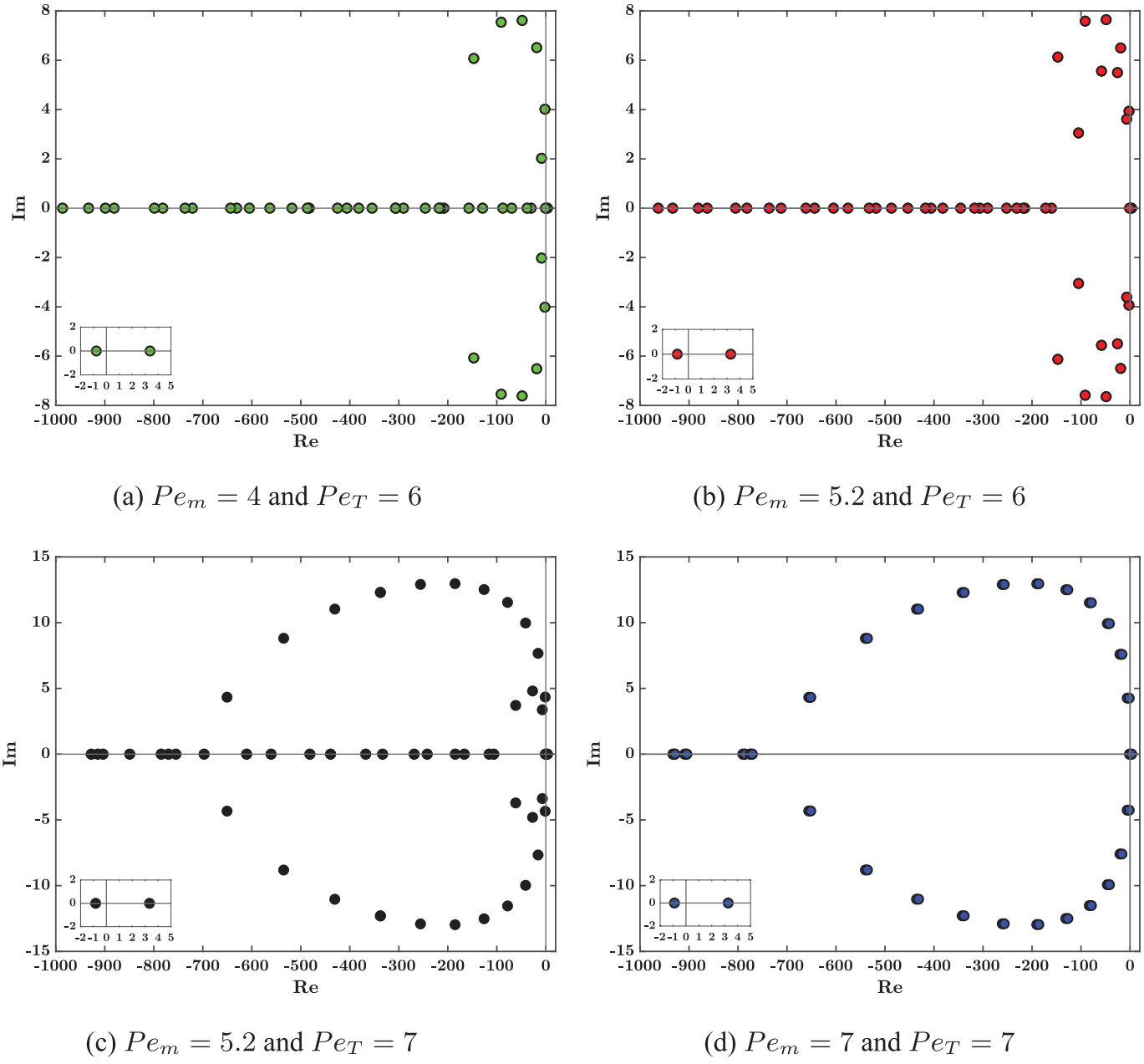

(a) $Pe_m = 4$ and $Pe_T = 6$ (b) $Pe_m = 5.2$ and $Pe_T = 6$

(c) $Pe_m = 5.2$ and $Pe_T = 7$ (d) $Pe_m = 7$ and $Pe_T = 7$

Fig. 3. Comparison of the eigenvalues' distribution with different setting for Peclet numbers.

5. Cayley-Tustin time discretization

5.1. Discrete time representation

In this subsection, for the mentioned coupled convection-diffusion parabolic PDEs, mapping the continuous time setting to discrete one is considered by the application of the Cayley-Tustin time discretization method. Let us consider Δt as the sampling time, then by applying Crank-Nicolson time discretization to Eq. (12), one can derive the following:

$$\frac{x(j\Delta t)-x((j-1)\Delta t)}{\Delta t} \approx A\frac{x(j\Delta t)+x((j-1)\Delta t)}{2} + Bu(j\Delta t),\ \ j \geq 1 \tag{25}$$

$$y(j\Delta t) \approx C\frac{x(k\Delta t)+x((k-1)\Delta t)}{2} + Du(k\Delta t),\ \ j \geq 1 \tag{26}$$

Next, we consider $u(j\Delta t)/\sqrt{\Delta t}$ as the approximation of $u(j\Delta t)$, and the convergence of $u(j\Delta t)/\sqrt{\Delta t}$ to $u(j\Delta t)$ as $\Delta t \to 0$ can be verified in several ways, similarly for $y(j\Delta t)$, see V.Havu and Malinen (2007). Accordingly, the following finite dimensional discrete time dynamics can be achieved, which is known as the Tustin transform (Franklin et al., 1998) in digital control framework:

$$\frac{x(j\Delta t)-x((j-1)\Delta t)}{\Delta t} \approx A\frac{x(j\Delta t)+x((j-1)\Delta t)}{2} + B\frac{u(j\Delta t)}{\sqrt{\Delta t}},\ \ j \geq 1 \tag{27}$$

$$\frac{y(j\Delta t)}{\sqrt{\Delta t}} \approx C\frac{x(j\Delta t)+x((j-1)\Delta t)}{2} + D\frac{u(j\Delta t)}{\sqrt{\Delta t}},\ \ j \geq 1 \tag{28}$$

By simple manipulation, and assuming a piecewise constant input within time intervals, the discrete time counter part of Eqs. (12) takes the following form:

$$\begin{aligned} x(\zeta, k) &= A_d x(\zeta, k-1) + B_d u(k) \\ y(k) &= C_d x(\zeta, k-1) + D_d u(k) \end{aligned} \tag{29}$$

with $\alpha = 2/\Delta t$ and the discrete spatial operators (A_d, B_d, C_d, D_d) given as:

$$\begin{bmatrix} A_d & B_d \\ C_d & D_d \end{bmatrix} = \begin{bmatrix} -I + 2\alpha[\alpha I - A]^{-1} & \sqrt{2\alpha}[\alpha I - A]^{-1}B \\ \sqrt{2\alpha}C[\alpha I - A]^{-1} & C[\alpha I - A]^{-1}B \end{bmatrix} \tag{30}$$

$\mathfrak{R}(s, A) = (sI - A)^{-1}$ and $(sI - A)^{-1}B = \mathfrak{R}(s, A)B$ are defined as the resolvent operators for A and B, respectively. In the above expression, it is important to emphasize that the original model expressed by Eq. (12) does not have a feedthrough operator while the discrete system Eq. (29) poses a well-defined feedthrough operator that is realized as transfer function, $D_d = G(\alpha) = C[\alpha - A]^{-1}B$, and includes a one to one relation between continuous and discrete setting (V.Havu and Malinen, 2007; Xu and Dubljevic, 2017). The physically realizable distributed parameter systems generally do not contain a feedforward operator ($D = 0$). This implies G(α) is strictly proper and does not involve instantaneous transfer from the input signal to the output one, such that G(α) is defined as a function evaluated at $s = \alpha$.

Remark 2. The Crank-Nicolson is a type of discretization scheme derived from the implicit midpoint rule and preserves the system's dynamical properties (stability, observability and controllability). This method of discretization is also referred to as the lowest order symplectic integration algorithm in Gauss quadrature based Runge-Kutta methods (Hairer et al., 2006).

5.2. Resolvents and discrete operators

The resolvent operator $\mathfrak{R}(s, A) = (sI - A)^{-1}$ of the operator A can be obtained by considering the system with a zero input condition which yields:

$$\mathfrak{R}(s, A)(\cdot) = \begin{bmatrix} \mathfrak{R}_{11} & \mathfrak{R}_{12} \\ \mathfrak{R}_{21} & \mathfrak{R}_{22} \end{bmatrix} \begin{bmatrix} (\cdot)_1 \\ (\cdot)_2 \end{bmatrix} \tag{31}$$

Proof. All the resolvent operators can be directly found by applying the Laplace transform to the class of parabolic PDEs described by Eq. (11):

$$\frac{\partial}{\partial \zeta} \underbrace{\begin{bmatrix} x_1(\zeta, s) \\ \frac{\partial x_1(\zeta, s)}{\partial \zeta} \\ x_2(\zeta, s) \\ \frac{\partial x_2 \zeta, s)}{\partial \zeta} \end{bmatrix}}_{X(\zeta, s)} = \underbrace{\begin{bmatrix} 0 \\ -Pe_m x_1(\zeta, 0) \\ 0 \\ -Pe_T x_2(\zeta, 0) \end{bmatrix}}_{Z_1(\zeta, 0)} + \underbrace{\begin{bmatrix} 0 \\ 0 \\ 0 \\ -Pe_T \sigma u(s) \end{bmatrix}}_{Z_2(s)}$$
$$+ \underbrace{\begin{bmatrix} 0 & 1 & 0 & 0 \\ Pe_m(s - \bar{R}_1) & Pe_m & -Pe_m \bar{R}_2 & 0 \\ 0 & 0 & 0 & 1 \\ -Pe_T \delta \bar{R}_1 & 0 & Pe_T(s - \delta \bar{R}_2 + \sigma) & Pe_T \end{bmatrix}}_{P} \begin{bmatrix} x_1(\zeta, s) \\ \frac{\partial x_1(\zeta, s)}{\partial \zeta} \\ x_2(\zeta, s) \\ \frac{\partial x_2(\zeta, s)}{\partial \zeta} \end{bmatrix} \tag{32}$$

since the matrix P includes constant variables, one can obtain the general solution as:

$$X(\zeta, s) = TX(0, s) + \int_0^{\zeta} FZ_1(\eta, 0)d\eta + \int_0^{\zeta} FZ_2(s)d\eta \tag{33}$$

which is the solution of the ODE given by Eq. (32). T and F are defined as 4×4 matrices, representing the exponential matrices $e^{P\zeta}$ and $e^{P(\zeta - \eta)}$, respectively. After some manipulation, the desired resolvent operator can be expressed as $\mathfrak{R}(s, A)(\cdot) = (sI - A)^{-1}(\cdot)$ involving four components, $\mathfrak{R}_{11}$, $\mathfrak{R}_{12}$, $\mathfrak{R}_{21}$, and $\mathfrak{R}_{22}$ constructed by the operators A_{11}, A_{12} A_{21} and A_{22} (see Appendix C.1 for details). □

Based on the discrete operators defined in the previous section and the resolvent in Eq. (31), the operator A_d can be written as the following convenient form:

$$A_d(\cdot) = -\begin{bmatrix} (\cdot)_1 \\ (\cdot)_2 \end{bmatrix} + 2\alpha \begin{bmatrix} \mathfrak{R}_{11} & \mathfrak{R}_{12} \\ \mathfrak{R}_{21} & \mathfrak{R}_{22} \end{bmatrix} \begin{bmatrix} (\cdot)_1 \\ (\cdot)_2 \end{bmatrix} \tag{34}$$

Similarly, one can obtain the operator B_d by using the resolvent operator $\mathfrak{R}(s, A)B = (sI - A)^{-1}B$, which can be computed by imposing zero initial condition ($X(\zeta = 0, s) = 0$) in Eq. (32). This leads to the following expression (see Appendix C.1):

$$B_d = \sqrt{2\alpha}\mathfrak{R}(\alpha, A)B = \begin{bmatrix} \mathfrak{R}_1 B \\ \mathfrak{R}_2 B \end{bmatrix} \tag{35}$$

According to Eq. (30) and the definition of the operators B and C presented in Section 3.2, the discrete operators C_d and D_d can be expressed as:

$$C_d(\cdot) = \sqrt{2\alpha}C\mathfrak{R}(\alpha, A)(\cdot) = \begin{bmatrix} \mathfrak{R}_{21}\big|_{\zeta=1} & \mathfrak{R}_{22}\big|_{\zeta=1} \end{bmatrix} \begin{bmatrix} (\cdot)_1 \\ (\cdot)_2 \end{bmatrix},$$
$$D_d = C\mathfrak{R}(\alpha, A)B = (\mathfrak{R}_2 B)\big|_{\zeta=1} \tag{36}$$

5.3. Resolvents of the adjoints and corresponding discrete operators

In order to design the model predictive control, the adjoint operators (A_d^*, B_d^*) are required, as well, in the controller design. Hence, in a similar manner described in the previous subsection, the expressions for the corresponding adjoint resolvent operators can be found by applying the Laplace transform on the adjoint system given by Eqs. (21) and (22):

$$\mathfrak{R}(\alpha, A^*)(\cdot) = \begin{bmatrix} \mathfrak{R}_{11}^* & \mathfrak{R}_{12}^* \\ \mathfrak{R}_{21}^* & \mathfrak{R}_{22}^* \end{bmatrix} \begin{bmatrix} (\cdot)_1 \\ (\cdot)_2 \end{bmatrix} \tag{37}$$

This yields the final form of the operator A_d^* given by:

$$A_d^*(\cdot) = -\begin{bmatrix} (\cdot)_1 \\ (\cdot)_2 \end{bmatrix} + 2\alpha \begin{bmatrix} \mathfrak{R}_{11}^* & \mathfrak{R}_{12}^* \\ \mathfrak{R}_{21}^* & \mathfrak{R}_{22}^* \end{bmatrix} \begin{bmatrix} (\cdot)_1 \\ (\cdot)_2 \end{bmatrix} \tag{38}$$

and one can construct the discrete operator B_d^* as below:

$$B_d^*(\cdot) = \sqrt{2\alpha}(\mathfrak{R}(\alpha, A)B)^*(\cdot) = \begin{bmatrix} (\mathfrak{R}_1 B)^* \\ (\mathfrak{R}_2 B)^* \end{bmatrix}^T \begin{bmatrix} (\cdot)_1 \\ (\cdot)_2 \end{bmatrix} \tag{39}$$

All the expressions of the resolvent components are provided in Appendix C.2.

6. Observer design for coupled parabolic PDEs

To address the issue of having access to all the state variables, the discrete output observer is considered in this work. The Luenberger observer is one of the practical and easy to realize observers, which is considered in a discrete modern controller realizations. However, the discrete operators cannot be directly used in calculating the observer gain in discrete-time setting. Therefore, the design is performed first in the continuous time setting. Then, the discrete observer gain is obtained from the continuous one by utilizing the Cayley-Tustin discretization scheme, which provides the link between stabilizing observer gains in continuous and discrete settings.

6.1. Design for the continuous-time observer

For the state reconstruction of the transport distributed parameter systems, particularly for the class of diffusion-convection-reaction parabolic PDEs, one can consider the following general representation without the feedforward term (i.e., D):

$$\begin{aligned} \dot{x}(\zeta, t) &= Ax(\zeta, t) + Bu(t) \\ y(t) &= Cx(\zeta, t) \end{aligned} \tag{40}$$

and the Luenberger observer can be presented by the following standard form:

$$\begin{aligned}\dot{\hat{x}}(\zeta,t) &= A\hat{x}(\zeta,t) + Bu(t) + L_T[y(t) - \hat{y}(t)]\\ \hat{y}(t) &= C\hat{x}(\zeta,t)\end{aligned} \tag{41}$$

where the reconstructed state $\hat{x}(\zeta,t)$ is defined as a copy of the system dynamics and considers the output of the plant provided in an affine manner. By subtracting Eq. (41) from its general form Eq. (40) and defining the observer error by $\hat{e}(\zeta,t) = x(\zeta,t) - \hat{x}(\zeta,t)$, yields the below expression:

$$\dot{\hat{e}}(\zeta,t) = (A - L_T C)\hat{e}(t) = A_o\hat{e}(\zeta,t) \tag{42}$$

the above design relies on choosing the appropriate spatially varying gain $L_T(\zeta) = \begin{bmatrix} L_1(\zeta) \\ L_2(\zeta) \end{bmatrix}$ such that the operator A_o in the state estimation error dynamics given by Eq. (42) is stable. Therefore, to ensure the stability of the observer, one can analyze the corresponding eigenvalues of Eq. (42):

$$A_o\phi_o = \lambda_o\phi_o \tag{43}$$

By the same method explained in Section 4, after imposing the boundary conditions, the eigenvalue problem for the operator A_o leads to a set of numerically solvable nonlinear equations. The design objective is to determine the observer's region of stability by considering the proper value for the observer gain, which is achieved by ensuring that all eigenvalues have negative real parts. Hence, one can consider various spatial functions $L_T(\zeta)$ in order to guarantee that eigenvalue problem in Eq. (43) provides stable error dynamics. Subsequently, once the observer gain is determined one needs to link this spatial gain to the corresponding discrete gain $L_d(\zeta)$. The relation between the continuous and discrete observer gain is provided in the ensuing section.

Remark 3. It can be proven that, as the eigenfunctions are nonzero at the measuring point ($C\hat{\Phi}_n = \hat{\Phi}_n(\zeta = 1) \neq 0$), the sum $\sum_{n=1}^{N} < x, \hat{\Phi}_{n_j} > C\hat{\Phi}_{n_j} \neq 0$. Hence the system is observable and one can find an observer gain L_T that guarantees the exponential stability of the operator A_o, as shown in Curtain and Zwart (1995); Xu and Dubljevic (2016).

6.2. Design for the discrete-time observer

A discrete version of the observer, similar to the discrete version of the plant model, is constructed as follows:

$$\begin{aligned}\hat{x}(\zeta,k) &= A_d\hat{x}(\zeta,k-1) + B_d u(k) + L_d[y(k) - \hat{y}(k)]\\ \hat{y}(k) &= C_{d_o}\hat{x}(\zeta,k-1) + D_{d_o}u(k) + M_{d_o}y(k)\end{aligned} \tag{44}$$

where A_d and B_d have been defined in Eq. (30). The other discrete operators, (C_{d_o}, D_{d_o}, L_d, M_{d_o}), are given as:

$$\begin{aligned}C_{d_o}(\cdot) &= \sqrt{2\alpha}[I + C(\alpha I - A)L_T]^{-1}C[\alpha I - A]^{-1}(\cdot)\\ D_{d_o} &= [I + C(\alpha I - A)L_T]^{-1}C[\alpha I - A]^{-1}B\\ M_{d_o} &= \left(I + C(\alpha I - A)^{-1}L_T\right)^{-1}C(\alpha I - A)^{-1}L_T\\ L_d &= \sqrt{2\alpha}[\alpha I - A]^{-1}L_T\end{aligned} \tag{45}$$

notice that L_d has similar structure to B_d, as y_k can be determined as an input to the observer.

Lemma 1. *If the continuous observer gain (L_T) is chosen such that (A_o) is stable, then the discrete version of the observer in Eq. (44) is stable as well. In other words, the Cayley-Tustin time discretization will preserve the system properties.*

Proof. In order to show the states constructed by observer will converge to the system state, one can realize the discrete observer error dynamics as:

$$\hat{e}_d(\zeta,k) = x(\zeta,k) - \hat{x}(\zeta,k) \tag{46}$$

and by some algebraic manipulation (see Appendix E), the relation between discrete and continuous setting is obtained and leads to the following form of the discrete error:

$$\begin{aligned}\hat{e}_d(\zeta,k) &= (A_d - L_d C_d)\hat{e}_d(\zeta,k-1)\\ &= \left(-I + 2[\alpha I - A + L_T C]^{-1}\right)\hat{e}_d(\zeta,k-1)\end{aligned} \tag{47}$$

□

where $\left(-I + 2[\alpha I - A + L_T C]^{-1}\right)$ is the discrete representation of $A_o = (A - L_T C)$. Thus, if the continuous observer gain (L_T) is chosen such that (A_o) is stable, then the proposed discrete observer is able to reconstruct the states, as A_o generates a stable discrete representation if the Cayley-Tustin time discretization is applied.

It should be mentioned that the presented methodology does not involve any model reduction associated with the discrete Luenberger observer design, and no spatial approximation has been considered compared to the spatial discretization schemes mainly used in the literature, see Dochain (2001, 2000); Mohd Ali et al. (2015); Alonso et al. (2004); Bitzer and Zeitz (2002).

7. Model predictive control for unstable coupled parabolic PDEs

This section addresses the design of the proposed model predictive controller for the coupled parabolic PDEs. The discrete-time model dynamics with eigenfunctions of the system are used to find the solution of the optimization problem.

7.1. Optimization problem

In this subsection, based on the scheme given in Fig. 4, the MPC design is developed for the infinite dimensional setting. As can be seen, the full state feedback is used by the MPC scheme, which will be estimated by the observer. The design of the regulator is emerged from the finite dimensional linear time invariant systems, see Rawlings et al. (2017).

Here, the following open-loop objective function is utilized as a foundation of a controller design providing minimization at each sampling time (k):

$$\begin{aligned}&\min_{u^N} \sum_{l=0}^{\infty} < \hat{x}(\zeta,k+l|k), Q\hat{x}(\zeta,k+l|k) >\\ &+ < u(k+l+1|k), Fu(k+l+1|k) >\\ &\text{s.t. } \hat{x}(\zeta,k+l|k) = A_d\hat{x}(\zeta,k+l-1|k) + B_d u(k+l|k),\\ &\quad u^{\min} \leqslant u(k+l|k) \leqslant u^{\max},\\ &\quad \hat{x}^{\min} \leqslant \hat{x}(\zeta=\zeta_c,k+l|k) \leqslant \hat{x}^{\max},\\ &\quad < \hat{x}(\zeta,k+N), \hat{\Phi}_u >= 0\end{aligned} \tag{48}$$

where $\hat{x}(\zeta,k) = \begin{bmatrix}\hat{x}_1(\zeta,k) & \hat{x}_2(\zeta,k)\end{bmatrix}^T$ indicates the state variables of the system, F is a positive definite operator, $Q = \begin{bmatrix} Q_1(\zeta) & 0 \\ 0 & Q_2(\zeta) \end{bmatrix}$ responsible for positive semidefinite spatial operator associated with the state of coupled parabolic PDEs, $(k+l)$ and $(k+l+1|k)$ are considered for current and future time, respectively. By assigning zero-input beyond the control horizon ($u(k \geq N+1|k) = 0$), the aforementioned infinite horizon objective function can be cast as the following finite horizon version (i.e,

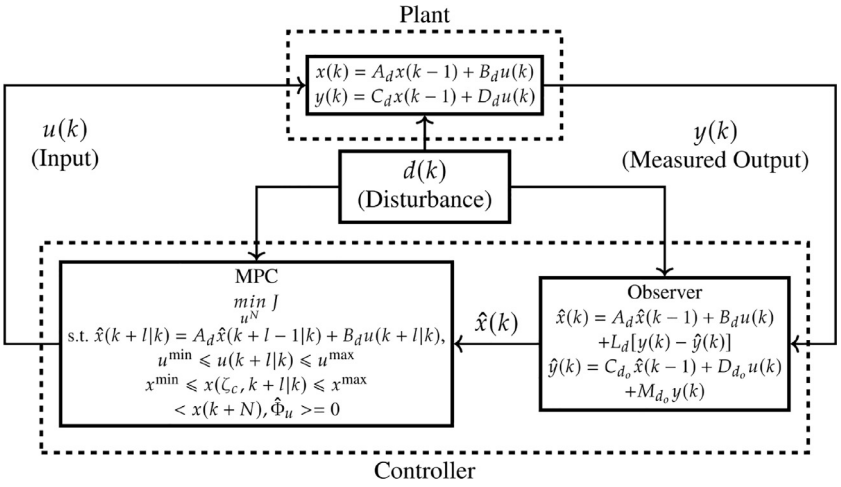

Fig. 4. Scheme of the model predictive controller used for the non-isothermal axial dispersion tubular reactor with recycle stream.

N-horizon length):

$$\begin{aligned}\min_{u^N} J = &\sum_{l=0}^{N-1} < \hat{x}(\zeta, k+l|k), Q\hat{x}(\zeta, k+l|k) > \\ &+ < u(k+l+1|k), Fu(k+l+1|k) > \\ &+ < \hat{x}(\zeta, k+N|k), \overline{Q}\hat{x}(\zeta, k+N|k) >\end{aligned} \tag{49}$$

$$\begin{aligned}\text{s.t. } &\hat{x}(\zeta, k+l|k) = A_d\hat{x}(\zeta, k+l-1|k) + B_d u(k+l|k), \\ &u^{\min} \leqslant u(k+l|k) \leqslant u^{\max}, \\ &\hat{x}^{\min} \leqslant \hat{x}(\zeta = \zeta_c, k+l|k) \leqslant \hat{x}^{\max}, \\ &< \hat{x}(\zeta, k+N), \hat{\Phi}_u >= 0\end{aligned}$$

where $\overline{Q}$ is obtained as the following terminal cost operator for the system of coupled parabolic PDEs (see Appendix D):

$$\overline{Q}(\cdot) = \sum_{m=0}^{\infty}\sum_{n=0}^{\infty} \frac{- < \hat{\Phi}_m, Q\hat{\Phi}_n^* >}{\lambda_m + \lambda_n} < (\cdot), \hat{\Phi}_n^* > \hat{\Phi}_m \tag{50}$$

Remark 4. If only stable modes with negative eigenvalues ($Re(\lambda) < 0$) are present, $\overline{Q}$ in Eq. (50) is a positive definite operator as Q is a nonnegative spatial operator. In order to handle the unstable modes with positive eigenvalues ($Re(\lambda) > 0$), the equality constraint is employed in the optimization problem. Therefore, if there is a feasible input sequence that satisfy such constraint, there will be no contributions of the unstable modes in Eq. (50) and $\overline{Q}$ will be a positive operator. In other words, the states will be in a stable sub-space where the stability is ensured (Xu and Dubljevic, 2017).

Regarding the equality constraint ($< \hat{x}(\zeta, k+N), \hat{\Phi}_u >= 0$), the following equation needs to be integrated in the convex optimization problem presented by Eq. (49):

$$\begin{aligned}&\left[< A_d^{N-1}B_d, \hat{\Phi}_u > \quad < A_d^{N-2}B_d, \hat{\Phi}_u > \quad \dots \quad < B_d, \hat{\Phi}_u >\right]U \\ &= - < A_d^N\hat{x}(\zeta, k|k), \hat{\Phi}_u >\end{aligned} \tag{51}$$

where $\hat{\Phi}_u$ is described as the relevant normalized unstable eigenfunctions associated with positive eigenvalues. Therefore, with feasible input sequence given by optimization problem, the equality constraint is satisfied and the unstable modes will be canceled at the end of the horizon.

By straightforward algebraic manipulation, one can express the objective function in Eq. (49) as the following quadratic optimization form:

$$\min_U \; J = 2U^T < I, P\hat{x}(\zeta, k|k) > + U^T < I, H > U + < \hat{x}(\zeta, k|k), \overline{Q}\hat{x}(\zeta, k|k) > \tag{52a}$$

which is subjected to the following constraints:

$$\begin{aligned}&U^{\min} \leqslant U \leqslant U^{\max} \\ &\hat{x}^{\min} \leqslant \left[SU + T\hat{x}(\zeta, k|k)\right]\Big|_{\zeta=\zeta_c} \leqslant \hat{x}^{\max} \\ &S_u U + T_u\hat{x}(\zeta, k|k) = 0\end{aligned} \tag{52b}$$

with:

$$H = \begin{bmatrix} B_d^*\overline{Q}B_d + F & B_d^*A_d^*\overline{Q}B_d & \dots & B_d^*A_d^{*N-1}\overline{Q}B_d \\ B_d^*\overline{Q}A_dB_d & B_d^*\overline{Q}B_d + F & \dots & B_d^*A_d^{*N-2}\overline{Q}B_d \\ \vdots & \vdots & \ddots & \vdots \\ B_d^*\overline{Q}A_d^{N-1}B_d & B_d^*\overline{Q}A_d^{N-2}B_d & \dots & B_d^*\overline{Q}B_d + F \end{bmatrix},$$

$$P = \begin{bmatrix} B_d^*\overline{Q}A_d \\ B_d^*\overline{Q}A_d^2 \\ \vdots \\ B_d^*\overline{Q}A_d^N \end{bmatrix}, \; T = \begin{bmatrix} A_d \\ A_d^2 \\ \vdots \\ A_d^N \end{bmatrix}, S = \begin{bmatrix} B_d & 0 & \dots & 0 \\ A_dB_d & B_d & \dots & 0 \\ \vdots & \vdots & \ddots & \vdots \\ A_d^{N-1}B_d & A_d^{N-2}B_d & \dots & B_d \end{bmatrix},$$

$$T_u = \begin{bmatrix} A_d \end{bmatrix}, \; S_u = \begin{bmatrix} A_d^{N-1}B_d & A_d^{N-2}B_d & \dots & B_d \end{bmatrix},$$

$$U = \begin{bmatrix} u(k+1|k) & u(k+2|k) & u(k+3|k) & \dots & u(k+N|k) \end{bmatrix}^T \tag{53}$$

The above standard formulation of the quadratic optimization problem leads to finite-dimensional quadratic programming with linear constraints. If feasible, then the constraints and optimality are fulfilled while the controller ensures the system stabilization.

7.2. Input disturbance rejection

In the chemical plant demonstrated in Fig. 1, heating/cooling jacket may involve possible temperature disturbance. To address this issue, in this subsection we implement the disturbance rejection based on the optimization problem discussed earlier. The axial dispersion tubular reactor system with recycle is a coupled parabolic PDEs system, which can be rewritten as:

$$\begin{aligned}\dot{x}(\zeta, t) &= Ax(\zeta, t) + B\tilde{u}(t) \\ y(t) &= Cx(\zeta, t)\end{aligned} \tag{54}$$

where $\tilde{u}(k)$ defined as the input variable with possible disturbance and given by:

$$\tilde{u}(t) = u(t) + d(t) \tag{55}$$

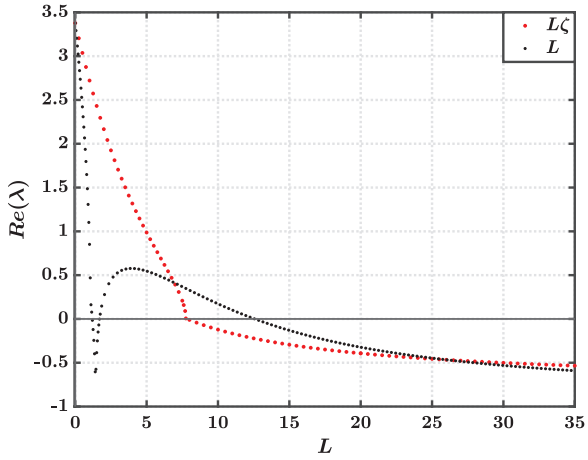

Fig. 5. Transition of the unstable eigenvalue to stable one by increasing the values for L as a constant valued function $(L_1(\zeta) = L_2(\zeta) = L)$ and a spatially varying function $(L_1(\zeta) = L_2(\zeta) = \zeta L)$ for the observer gains.

Then, the reformulated discrete version of the plant can be written as below:

$$\begin{aligned} x(\zeta, k) &= A_d x(\zeta, k-1) + B_d \tilde{u}(k) \\ y(k) &= C_d x(\zeta, k-1) + D_d \tilde{u}(k) \end{aligned} \tag{56}$$

Based on the optimization problem given by Eq. (48), in a similar manner and by substitution input $u(k)$ with the aforementioned manipulated variable $\tilde{u}(k)$, one can obtain the following new quadratic form of the objective function:

$$\begin{aligned} &\min_U \; J = 2U^T \left[< I, P\hat{x}(\zeta, k|k) > + < I, FG > \right] + U^T < I, H > U \\ &+ < \hat{x}(\zeta, k|k), \overline{Q}\hat{x}(\zeta, k|k) > + < G, FG > \\ &\text{s.t.} \quad U^{\min} \leqslant U + G \leqslant U^{\max} \\ &\hat{x}^{\min} \leqslant \left[S(U+G) + T\hat{x}(\zeta, k|k) \right] \Big|_{\zeta=\zeta_c} \leqslant \hat{x}^{\max} \\ &S_u(U+G) + T_u \hat{x}(\zeta, k|k) = 0 \end{aligned} \tag{57}$$

where U and the operators H, P, T, T_u, S, and S_u have been defined previously. G is defined as:

$$G = \begin{bmatrix} d(k+1|k) & d(k+2|k) & d(k+3|k) & \dots & d(k+N|k) \end{bmatrix}^T \tag{58}$$

Therefore, with feasible input, the proposed constrained optimization problem can also be accounted for input disturbance rejection.

8. Simulation results

This section is dedicated to the implementation of the model predictive controller for the axial dispersion tubular reactor with recycle, see the scheme in Fig. 4. The particular choice of parameters given by Table 1 leads to three equilibria for the system as shown in Fig. 2. The outer two profiles are stable, while the middle one is unstable and will be considered in the simulation study. Based on the model predictive control designed in Section 7, our objective is to stabilize the system while complying with input/state constraints. The developed controller can also address the issue of having possible known input disturbance in the system. Due to the construction of the optimization problem, as discussed in Section 4, one can perform the eigenvalue problem to calculate the eigenvalues, eigenfunctions, and adjoint eigenfunctions for the unstable coupled parabolic PDEs system.

Table 1
Values of the parameters used in numerical simulations.

Variable	Value	Unit
Pe_m	4	–
Pe_T	6	–
k_a	0.6	–
δ	0.8	–
σ	0.9	–
r	0.3	–
η	20	–
T_{Feed}	600	K
$C_{A_{Feed}}$	1	$\frac{\text{mol}}{\text{l}}$
$T_{w_{ss}}$	380	K

Based on Fig. 4, the discrete observer is considered in the close-loop setting. As discussed in Section 6, the stability of the observer is evaluated by the analysis of observer error dynamics. Thus, the corresponding eigenvalue problem in Eq. (43) is studied for increasing values of the observer gains. Two cases are investigated: one provides a constant value for the observer gain in the entire spatial domain (L); the other considers a linear spatially varying function $(L(\zeta) = L\zeta)$ for the mentioned observer gain. In general, one can propose different types of the spatial functions $L(\zeta)$ and calculate the region of stability by considering Eq. (43).

Subsequently, in order to have a better realization of the proposed design, the most positive eigenvalue for each gain is extracted and shown in Fig. 5. From Fig. 5, it can be seen that, for the case with $L_1(\zeta) = L_2(\zeta) = L$, as the value of the gain is increased, the unstable eigenvalue is shifted to the left side of the complex plain, while at the same time increasing gain leads to the shift of the stable pair of the eigenvalues to the right half plane, making the observer error dynamics unstable again. Hence, the stability region for this observer design refers to $1.20 \leq L \leq 1.70$ and $12.60 \leq L \leq 35$, while for the second case, the desired stability region is $7.85 \leq L \leq 35$.

We show simulation studies of observer for a model of an axial dispersion tubular reactor with recycle. The gain $L = 24$ is chosen as the constant observer gain in the whole spatial domain and the related discrete version is computed based on Eq. (45). Considering zero initial condition for the observer dynamics, the equivalent discrete error dynamic written in Eq. (47) is evaluated and shown in Fig. 6. It can be confirmed that the error dynamics is decaying exponentially such that the stability of the observer is guaranteed.

Based on the developed observer, one can use Eq. (44) to obtain the reconstructed states in the discrete-time setting for both temperature and concentration through the dispersive tubular reactor. In numerical simulation, $x_0(\zeta)$ belongs to the domain of A, $\Delta t = 0.04$ that implies $\alpha = 50$ and $\Delta z = 0.005$ for numerical integration. Next, the normalized eigenfunctions of the system with corresponding biorthonormal ones are used to determine the terminal cost operator presented in Eq. (50). The manipulation of the MPC is obtained by the application of the constrained optimization problem (see Eqs. (48)–(53)) on the basis of Cayley-Tustin time discretization with $Qx = 2x$, $F = 0.2$ and $N = 10$ as the control horizon. From Fig. 7, it is possible to verify that the close-loop system under model predictive control is successful in stabilizing the unstable mode at end of the horizon and satisfies the stability constraint for the system of coupled parabolic PDEs.

As emphasized in Section 7.2, in this chemical plant, tuning the temperature of the wall may involve possible temperature disturbance. In this work, we consider a square wave function as the known disturbance with period of three time steps and an amplitude of $20K$ injected into the system. Based on the quadratic optimization problem stated in Eq. (57) and the scheme given by

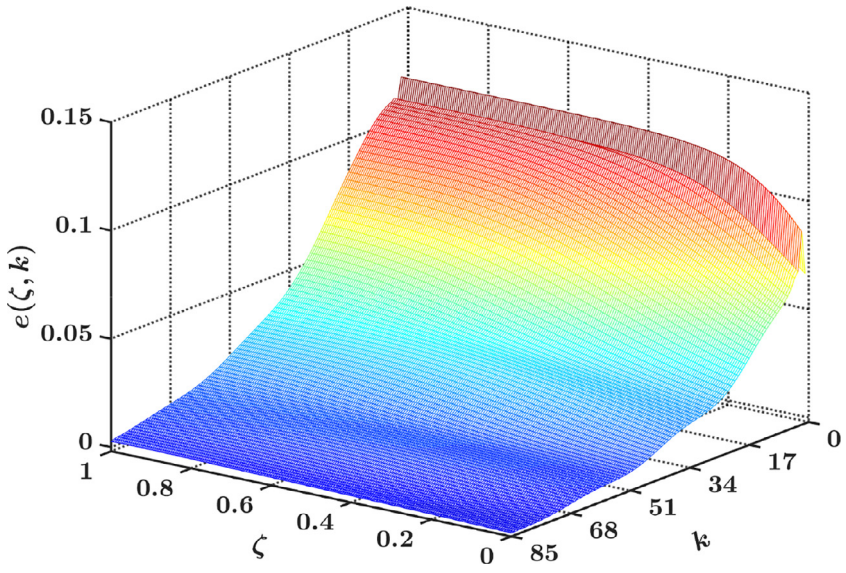

Fig. 6. Discrete observer error dynamics given by Eq. (47) with $L = 24$.

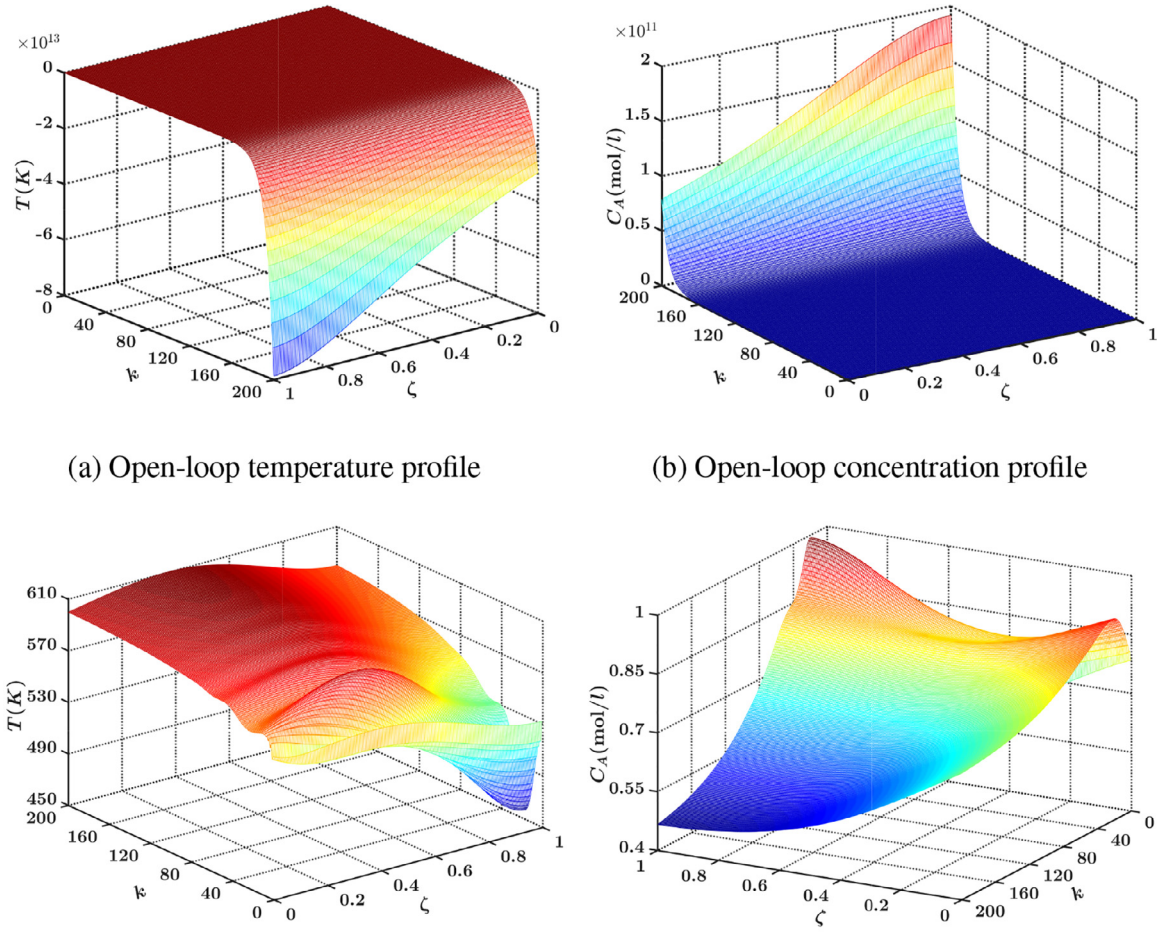

Fig. 7. Dynamics reconstruction of the spatial profiles for the axial dispersion tubular reactor constructed on the basis of a discrete time parabolic PDEs system in an open-loop/close-loop condition.

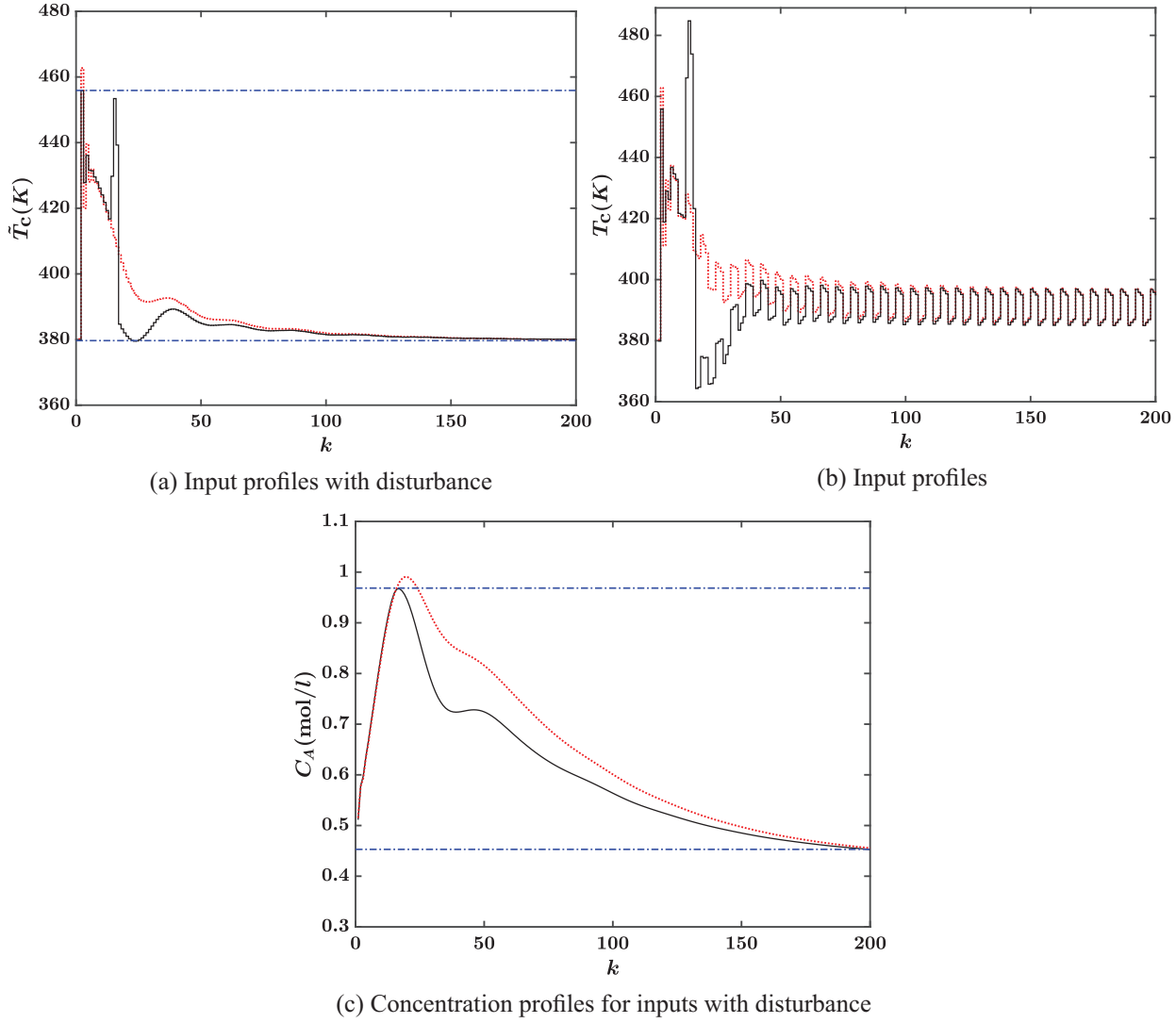

Fig. 8. Comparison between inputs with square wave disturbance $\tilde{T}_c$, controlled inputs T_c and concentration profiles under model predictive controller subjected to all constraints (solid-lines) or only stability constraint (dotted lines).

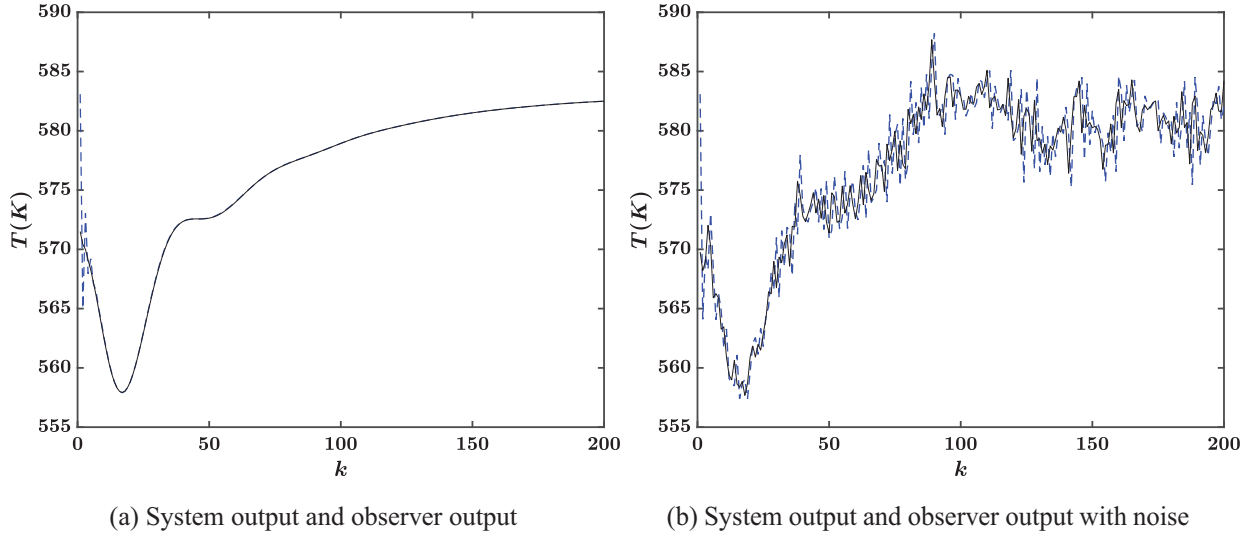

Fig. 9. Comparison of the system output (solid lines) and observer output (dashed lines) with and without measurement noise in the non-isothermal tubular reactor under the model predictive control and using the Luenberger observer in Eq. (44).

Fig. 4, two scenarios are justified in the simulation study. For the first one, all the constraints (stability, state and input) with the input disturbance are assigned to the objective function. However, in the latter case, MPC is only subjected to stabilizing the coupled parabolic PDEs with consideration of input disturbance. From Fig. 8(a), it can be seen that the input with disturbance while all constraints are activated, can satisfy the upper and lower limitations of manipulated input variable compared to the second scenario that only the stability constraint is applied on the system. The related controlled actions with respect to disturbance rejection are presented in Fig. 8(b).

Moreover, in a realistic physical systems various cases can be considered as the points where state constraints can be imposed. For example, the reactor outlet concentration, or the temperature constraint along the reactor to account with any hot spots generated throughout the axial dispersion reactor. Here, the concentration of the component at end of the chemical tubular reactor ($\zeta = 1$) is introduced as the state constraint in the MPC controller. The result for corresponding state limitation is demonstrated in Fig. 8(c) according to the input manipulations.

In a chemical process, the noise originating from operational environment may also affect the close-loop system. Thus, another case study is considered, such that measurement noise is included in the system output (temperature at reactor outlet). Fig. 9 gives the simulation result for the system output with measurement noise, which is modelled as a white noise with standard variance $\kappa = 0.05$ and zero mean. As it is possible to notice, the model predictive controller is able to maintain the operation of the non-isothermal axial dispersion reactor at the desired steady state.

Based on the above simulation studies, it is possible to see that the developed constrained optimal controller can provide system stabilization, complying with constraints and reject the possible input disturbance. In addition, the observer reconstructs the states of the dispersive tubular reactor properly through the system output such that MPC is applicable in the chemical plant.

9. Conclusion

In this contribution, the design of a model predictive controller and discrete observer were investigated for an axial dispersion tubular reactor with recycle. The discrete version of the overall system is provided by the application of the Cayley-Tustin time discretization on the linearization of a coupled nonlinear convection-diffusion-reaction PDEs system. An unstable operating condition with different energy and mass Peclet numbers is considered for the tubular reactor. The discrete representation of the system is obtained without any model reduction or spatial approximation, while the system properties (such as controllability, observability and stability) are preserved. Besides the stabilizing condition given by a terminal constraint, the physical limitation of the process (state and input constraints) with possible disturbance in control manipulation were placed in the formulation of the constrained optimization problem. The simulation results demonstrated the good performance of the controller by regulating the cooling jacket temperature of the reactor. As expected, the system under the proposed model predictive controller was able to achieve stabilization and provide constraints satisfaction while rejecting the input disturbance. The proposed optimal control scheme with consideration of constraints is designed to help the chemical process to operate efficiently in accordance with the process limitations.

Declaration of Competing Interest

The authors declare that they have no known competing financial interests or personal relationships that could have appeared to influence the work reported in this paper.

CRediT authorship contribution statement

Seyedhamidreza Khatibi: Software, Writing - original draft, Writing - review & editing, Methodology. **Guilherme Ozorio Cassol:** Writing - review & editing, Methodology. **Stevan Dubljevic:** Writing - review & editing, Methodology, Supervision.

Acknowledgment

The support provided by CAPES - 88881.128514/2016-01 (Brazil) for Guilherme Ozorio Cassol is gratefully acknowledged.

Appendix A. Parameters of the non-isothermal axial dispersion tubular reactor with recycle

Table A1
Parameters of the chemical tubular reactor system used to model Eq. (1).

Variable	Unit	Description
l_r	m	Length of the tubular reactor
d_t	m	Diameter of the tubular reactor
R	kJ/kg K	Gas constant
λ	kJ/ms K	Axial energy dispersion coefficient
v	m/s	Fluid superficial velocity
D	m^2/s	Axial mass diffusivity
T_c	K	Jacket temperature
h	kJ/m^2 Ks	Heat transfer coefficient for wall
ρ_f	kg/m^3	Fluid density
C_p	kJ/kg K	Heat capacity of reacting fluid
E	kJ/kg	Activation energy
ΔH_r	kJ/kg	Heat of reaction*
r		Recycle ratio

* For endothermic reactions $\Delta H_r > 0$, and for exothermic reactions $\Delta H_r < 0$.

Appendix B. Finding adjoint operator and its boundary conditions

In order to find the adjoint operator A^* and its corresponding boundary conditions, one can use the following definition:

$$< A\Phi, \Psi >=< \Phi, A^*\Psi > \tag{B.1}$$

which leads to:

$$\left\langle \begin{bmatrix} A_{11} & A_{12} \\ A_{21} & A_{22} \end{bmatrix} \begin{bmatrix} \Phi_1 \\ \Phi_2 \end{bmatrix}, \begin{bmatrix} \Psi_1 \\ \Psi_2 \end{bmatrix} \right\rangle = \langle A_{11}\Phi_1, \Psi_1 \rangle + \langle A_{12}\Phi_2, \Psi_1 \rangle + \langle A_{21}\Phi_1, \Psi_2 \rangle + \langle A_{22}\Phi_2, \Psi_2 \rangle \tag{B.2}$$

where:

$$\begin{aligned} A_{11} &= \tfrac{1}{Pe_m}\tfrac{\partial^2}{\partial\zeta^2} - \tfrac{\partial}{\partial\zeta} + \overline{R}_1, \;\; A_{12} = \overline{R}_2 \\ A_{21} &= \delta\overline{R}_1, \;\; A_{22} = \tfrac{1}{Pe_T}\tfrac{\partial^2}{\partial\zeta^2} - \tfrac{\partial}{\partial\zeta} + (\delta\overline{R}_2 - \sigma) \end{aligned} \tag{B.3}$$

By employing integration by parts and some simple manipulations, one has:

$$
\begin{aligned}
&< A_{11}\Phi_1, \Psi_1 > + < A_{12}\Phi_2, \Psi_1 > + < A_{21}\Phi_1, \Psi_2 > + < A_{22}\Phi_2, \Psi_2 > \\
&= \tfrac{1}{Pe_m}\Psi_1(1)\tfrac{\partial\Phi_1}{\partial\zeta}\Big|_{\zeta=1} - \tfrac{1}{Pe_m}\Psi_1(0)\tfrac{\partial\Phi_1}{\partial\zeta}\Big|_{\zeta=0} - \tfrac{1}{Pe_m}\Phi_1(1)\tfrac{\partial\Psi_1}{\partial\zeta}\Big|_{\zeta=1} \\
&+ \tfrac{1}{Pe_m}\Phi_1(0)\tfrac{\partial\Psi_1}{\partial\zeta}\Big|_{\zeta=0} - \Phi_1(1)\Psi_1(1) + \Phi_1(0)\Psi_1(0) + \tfrac{1}{Pe_T}\Psi_2(1)\tfrac{\partial\Phi_2}{\partial\zeta}\Big|_{\zeta=1} \\
&- \tfrac{1}{Pe_T}\Psi_2(0)\tfrac{\partial\Phi_2}{\partial\zeta}\Big|_{\zeta=0} - \tfrac{1}{Pe_T}\Phi_2(1)\tfrac{\partial\Psi_2}{\partial\zeta}\Big|_{\zeta=1} + \tfrac{1}{Pe_T}\Phi_2(0)\tfrac{\partial\Psi_2}{\partial\zeta}\Big|_{\zeta=0} - \Phi_2(1) \\
&\Psi_2(1) + \Phi_2(0)\Psi_2(0) + \int_0^1 \left(\frac{1}{Pe_m}\Phi_1\frac{\partial^2\Psi_1}{\partial\zeta^2} + \Phi_1\frac{\partial\Psi_1}{\partial\zeta} + \bar{R}_1\Phi_1\Psi_1\right)d\zeta \\
&+ \int_0^1 \bar{R}_2\Phi_1\Psi_1 d\zeta + \int_0^1 \left(\frac{1}{Pe_T}\Phi_2\frac{\partial^2\Psi_2}{\partial\zeta^2} + \Phi_2\frac{\partial\Psi_2}{\partial\zeta} + (\delta\bar{R}_2 - \sigma)\Phi_2\Psi_2\right)d\zeta \\
&+ \int_0^1 \delta\bar{R}_1\Phi_1\Psi_2 d\zeta = < \Phi, A^*\Psi >
\end{aligned}
\tag{B.4}
$$

Then, injecting the boundary conditions given in Eq. (11), leads to the following new boundary conditions for the adjoint operator:

$$
\begin{aligned}
\tfrac{\partial\Psi_1(\zeta,t)}{\partial\zeta}\Big|_{\zeta=1} &= -Pe_m(\Psi_1(\zeta=1) - r\Psi_1(\zeta=0)) \\
\tfrac{\partial\Psi_2(\zeta,t)}{\partial\zeta}\Big|_{\zeta=1} &= -Pe_T(\Psi_2(\zeta=1) - r\Psi_2(\zeta=0)) \\
\tfrac{\partial\Psi_1(\zeta,t)}{\partial\zeta}\Big|_{\zeta=0} &= \tfrac{\partial\Psi_2(\zeta,t)}{\partial\zeta}\Big|_{\zeta=0} = 0
\end{aligned}
\tag{B.5}
$$

where the operators are given as:

$$
\begin{aligned}
A_{11}^* &= \tfrac{1}{Pe_m}\tfrac{\partial^2}{\partial\zeta^2} + \tfrac{\partial}{\partial\zeta} + \bar{R}_1,\ A_{12}^* = \delta\bar{R}_1 \\
A_{21}^* &= \bar{R}_2,\ A_{22}^* = \tfrac{1}{Pe_T}\tfrac{\partial^2}{\partial\zeta^2} + \tfrac{\partial}{\partial\zeta} + (\delta\bar{R}_2 - \sigma)
\end{aligned}
\tag{B.6}
$$

Appendix C. Resolvent operators

C1. Resolvent of the tubular reactor with recycle

The resolvent operator can be written as below:

$$
\mathfrak{R}(s,A)(\cdot) = \begin{bmatrix} \mathfrak{R}_{11} & \mathfrak{R}_{12} \\ \mathfrak{R}_{21} & \mathfrak{R}_{22} \end{bmatrix}\begin{bmatrix} (\cdot)_1 \\ (\cdot)_2 \end{bmatrix}
\tag{C.1}
$$

Considering $u(s) = 0$ and utilizing boundary conditions, one can find the followings:

$$
\begin{aligned}
\mathfrak{R}_{11} &= T_{1j}^{(\zeta)}(M_{ij}\gamma_i) - \int_0^\zeta \left(F_{12}^{(\zeta,\eta)}Pe_m(\cdot)_1\right)d\eta \\
\mathfrak{R}_{12} &= T_{1j}^{(\zeta)}(M_{ij}\Gamma_i) - \int_0^\zeta \left(F_{14}^{(\zeta,\eta)}Pe_T(\cdot)_2\right)d\eta \\
\mathfrak{R}_{21} &= T_{3j}^{(\zeta)}(M_{ij}\gamma_i) - \int_0^\zeta \left(F_{32}^{(\zeta,\eta)}Pe_m(\cdot)_1\right)d\eta \\
\mathfrak{R}_{22} &= T_{3j}^{(\zeta)}(M_{ij}\Gamma_i) - \int_0^\zeta \left(F_{34}^{(\zeta,\eta)}Pe_T(\cdot)_2\right)d\eta
\end{aligned}
\tag{C.2}
$$

with:

$$
M_{ij} = \begin{bmatrix} T_{21}^{(\zeta=1)} & T_{22}^{(\zeta=1)} & T_{23}^{(\zeta=1)} & T_{24}^{(\zeta=1)} \\ T_{41}^{(\zeta=1)} & T_{42}^{(\zeta=1)} & T_{43}^{(\zeta=1)} & T_{44}^{(\zeta=1)} \\ Pe_m(rT_{11}^{(\zeta=1)} - 1) & 1 + Pe_m rT_{12}^{(\zeta=1)} & Pe_m rT_{13}^{(\zeta=1)} & Pe_m rT_{14}^{(\zeta=1)} \\ Pe_T rT_{31}^{(\zeta=1)} & Pe_T rT_{32}^{(\zeta=1)} & Pe_T(rT_{33}^{(\zeta=1)} - 1) & 1 + Pe_T rT_{34}^{(\zeta=1)} \end{bmatrix}^{-1},
$$

$$
\gamma_i = \begin{bmatrix} \int_0^{\zeta=1}\left(F_{22}^{(\zeta=1,\eta)}Pe_m(\cdot)_1\right)d\eta \\ \int_0^{\zeta=1}\left(F_{42}^{(\zeta=1,\eta)}Pe_m(\cdot)_1\right)d\eta \\ Pe_m r\int_0^{\zeta=1}\left(F_{12}^{(\zeta=1,\eta)}Pe_m(\cdot)_1\right)d\eta \\ Pe_T r\int_0^{\zeta=1}\left(F_{32}^{(\zeta=1,\eta)}Pe_m(\cdot)_1\right)d\eta \end{bmatrix},
$$

$$
\Gamma_i = \begin{bmatrix} \int_0^{\zeta=1}\left(F_{24}^{(\zeta=1,\eta)}Pe_T(\cdot)_2\right)d\eta \\ \int_0^{\zeta=1}\left(F_{44}^{(\zeta=1,\eta)}Pe_T(\cdot)_2\right)d\eta \\ Pe_m r\int_0^{\zeta=1}\left(F_{14}^{(\zeta=1,\eta)}Pe_T(\cdot)_2\right)d\eta \\ Pe_T r\int_0^{\zeta=1}\left(F_{34}^{(\zeta=1,\eta)}Pe_T(\cdot)_2\right)d\eta \end{bmatrix}
\tag{C.3}
$$

for B_d, zero initial condition should be taken into account. This leads to the following resolvent:

$$
(sI - A)^{-1}B = \mathfrak{R}(s,A)B = \begin{bmatrix} \mathfrak{R}_1 B \\ \mathfrak{R}_2 B \end{bmatrix}
\tag{C.4}
$$

where

$$
\mathfrak{R}_1 B = T_{1j}^{(\zeta)}(M_{ij}\Omega_i) - \int_0^\zeta (F_{14}^{(\zeta,\eta)}Pe_T\sigma)d\eta
\tag{C.5}
$$

$$
\mathfrak{R}_2 B = T_{3j}^{(\zeta)}(M_{ij}\Omega_i) - \int_0^\zeta (F_{34}^{(\zeta,\eta)}Pe_T\sigma)d\eta
\tag{C.6}
$$

and Ω_i is defined as below:

$$
\Omega_i = \begin{bmatrix} \int_0^{\zeta=1}(F_{24}^{(\zeta=1,\eta)}Pe_T\sigma)d\eta \\ \int_0^{\zeta=1}(F_{44}^{(\zeta=1,\eta)}Pe_T\sigma)d\eta \\ Pe_m r\int_0^{\zeta=1}(F_{14}^{(\zeta=1,\eta)}Pe_T\sigma)d\eta \\ Pe_T r\int_0^{\zeta=1}(F_{34}^{(\zeta=1,\eta)}Pe_T\sigma)d\eta \end{bmatrix}
\tag{C.7}
$$

C2. Resolvent of adjoint operators

By the same procedure described in Section 5.2 for the operator A, consider T^* and F^* as the exponential matrices, $e^{P^*\zeta}$ and $e^{P^*(\zeta-\eta)}$, for the adjoint operator (A^*). This leads to the following resolvent by imposing the corresponding adjoint boundary conditions:

$$
\mathfrak{R}(s,A^*)(\cdot) = \begin{bmatrix} \mathfrak{R}_{11}^* & \mathfrak{R}_{12}^* \\ \mathfrak{R}_{21}^* & \mathfrak{R}_{22}^* \end{bmatrix}\begin{bmatrix} (\cdot)_1 \\ (\cdot)_2 \end{bmatrix}
\tag{C.8}
$$

where

$$
\begin{aligned}
\mathfrak{R}_{11}^* &= T_{11}^{*(\zeta)}(M_{1j}^*\gamma_j^*) + T_{13}^{*(\zeta)}(M_{2j}^*\gamma_j^*) - \int_0^\zeta \left(F_{12}^{*(\zeta,\eta)}Pe_m(\cdot)_1\right)d\eta \\
\mathfrak{R}_{12}^* &= T_{11}^{*(\zeta)}(M_{1j}^*\Gamma_j^*) + T_{13}^{*(\zeta)}(M_{2j}^*\Gamma_j^*) - \int_0^\zeta \left(F_{14}^{*(\zeta,\eta)}Pe_T(\cdot)_2\right)d\eta \\
\mathfrak{R}_{21}^* &= T_{31}^{*(\zeta)}(M_{1j}^*\gamma_j^*) + T_{33}^{*(\zeta)}(M_{2j}^*\gamma_j^*) - \int_0^\zeta \left(F_{32}^{*(\zeta,\eta)}Pe_m(\cdot)_1\right)d\eta \\
\mathfrak{R}_{22}^* &= T_{31}^{*(\zeta)}(M_{1j}^*\Gamma_j^*) + T_{33}^{*(\zeta)}(M_{2j}^*\Gamma_j^*) - \int_0^\zeta \left(F_{34}^{*(\zeta,\eta)}Pe_T(\cdot)_2\right)d\eta
\end{aligned}
\tag{C.9}
$$

and $(\gamma_i^*,\ \Gamma_i^*,\ M_{ij}^*)$ are expressed as:

$$\gamma_i^* = \begin{bmatrix} \int_0^{\zeta=1} \left(F_{22}^{*(\zeta=1,\eta)} Pe_m(\cdot)_1 + F_{12}^{*(\zeta=1,\eta)} Pe_m^2(\cdot)_1\right) d\eta \\ \int_0^{\zeta=1} \left(F_{42}^{*(\zeta=1,\eta)} Pe_m(\cdot)_1 d\eta + F_{32}^{*(\zeta=1,\eta)} Pe_m Pe_T(\cdot)_1\right) d\eta \end{bmatrix},$$

$$\Gamma_i^* = \begin{bmatrix} \int_0^{\zeta=1} \left(F_{24}^{*(\zeta=1,\eta)} Pe_T(\cdot)_2 + F_{14}^{*(\zeta=1,\eta)} Pe_m Pe_T(\cdot)_2\right) d\eta \\ \int_0^{\zeta=1} \left(F_{44}^{*(\zeta=1,\eta)} Pe_T(\cdot)_2 d\eta + F_{34}^{*(\zeta=1,\eta)} Pe_T^2(\cdot)_2\right) d\eta \end{bmatrix},$$

$$M_{ij}^* = \begin{bmatrix} T_{21}^{*(\zeta=1)} - Pe_m R + Pe_m T_{11}^{*(\zeta=1)} & T_{23}^{*(\zeta=1)} + Pe_m T_{13}^{*(\zeta=1)} \\ T_{41}^{*(\zeta=1)} + Pe_T T_{31}^{*(\zeta=1)} & T_{43}^{*(\zeta=1)} - Pe_T R + Pe_T T_{33}^{*(\zeta=1)} \end{bmatrix}^{-1} \tag{C.10}$$

Finally, for B_d^* it is possible to write:

$$(\mathfrak{R}_1 B)^*(\cdot)_1 = \int_0^1 (\mathfrak{R}_1 B)(\cdot)_1 d\zeta \tag{C.11}$$

$$(\mathfrak{R}_2 B)^*(\cdot)_2 = \int_0^1 (\mathfrak{R}_2 B)(\cdot)_2 d\zeta \tag{C.12}$$

Appendix D. Terminal cost operator

In this appendix, the algorithm for calculating the operator $\overline{Q}=\begin{bmatrix}\overline{Q}_1 & \overline{Q}_2\end{bmatrix}^T$ is demonstrated. Let us consider the following discrete Lyapunov equation:

$$A_d^* \overline{Q} A_d - \overline{Q} = -Q \tag{D.1}$$

Based on the Cayley-Tustin method, the solution of the above equation leads to the same unique solution in the continuous time setting $(A^*\overline{Q} + \overline{Q}A = -Q)$. The continuous Lyapunov equation can be formulated as the following inner product form (Curtain and Zwart, 1995):

$$< Ax_1, \overline{Q}x_2 > + < \overline{Q}x_1, Ax_2 > = - < x_1, Qx_2 > \tag{D.2}$$

Let us consider $x_1 = \hat{\Phi}_m$ and $x_2 = \hat{\Phi}_n^*$ as the normalized eigenfunctions and corresponding adjoint eigenfunctions of the operator A, respectively. The eigenvalue problem directly denotes that $A\hat{\Phi}_m = \lambda_m \hat{\Phi}_m$ and $A\hat{\Phi}_n^* = \lambda_n \hat{\Phi}_n^*$. Thus, the above equation leads to:

$$\begin{aligned} &< \lambda_m \hat{\Phi}_m, \overline{Q}\hat{\Phi}_n^* > + < \overline{Q}\hat{\Phi}_m, \lambda_n \hat{\Phi}_n^* > = \lambda_m < \hat{\Phi}_m, \overline{Q}\hat{\Phi}_n^* > \\ &+\lambda_n < \overline{Q}\hat{\Phi}_m, \hat{\Phi}_n^* > = - < \hat{\Phi}_m, Q\hat{\Phi}_n^* > \end{aligned} \tag{D.3}$$

where $\overline{Q}$ is a bounded symmetric operator $(D(A^*) = D(A))$ and it is self-adjoint, see Curtain and Zwart (1995). Therefore, $< \hat{\Phi}_m, \overline{Q}\hat{\Phi}_n^* > = < \overline{Q}\hat{\Phi}_m, \hat{\Phi}_n^* > = \overline{Q}_{mn}$ and it is possible to write the following simplified equation:

$$\overline{Q}_{mn} = \frac{- < \hat{\Phi}_m, Q\hat{\Phi}_n^* >}{\lambda_m + \lambda_n} \tag{D.4}$$

Finally, based on the solution of the continuous Lyapunov equation, the terminal cost operator can be computed by:

$$\overline{Q}(\cdot) = \sum_{m=0}^{\infty}\sum_{n=0}^{\infty} \frac{- < \hat{\Phi}_m, Q\hat{\Phi}_n^* >}{\lambda_m + \lambda_n} < (\cdot), \hat{\Phi}_n^* > \hat{\Phi}_m \tag{D.5}$$

Appendix E. Stability of the discrete error observer

First, we need to show that the discrete observer error can be written as the following equation:

$$\hat{e}_d(\zeta, k) = x(\zeta, k) - \hat{x}(\zeta, k) = (A_d - L_d C_d)\hat{e}_d(\zeta, k-1) \tag{E.1}$$

Let us recall that the discrete operators of the observer dynamics are given by:

$$\begin{aligned} &A_d(\cdot) = -I(\cdot) + 2\alpha[\alpha I - A]^{-1}(\cdot) \\ &B_d = \sqrt{2\alpha}[\alpha I - A]^{-1}B \\ &C_{d_o}(\cdot) = \sqrt{2\alpha}[I + C(\alpha I - A)L_T]^{-1}C[\alpha I - A]^{-1}(\cdot) \\ &D_{d_o} = [I + C(\alpha I - A)L_T]^{-1}C[\alpha I - A]^{-1}B \\ &M_{d_o} = (I + C(\alpha I - A)^{-1}L_T)^{-1}C(\alpha I - A)^{-1}L_T \\ &L_d = \sqrt{2\alpha}[\alpha I - A]^{-1}L_T \end{aligned} \tag{E.2}$$

Notice that in above equations M_{d_o} is defined according to L_T, such that the discrete observer error is stable. The relations between (C_{d_o}, D_{d_o}) and (C_d, D_d) are written as:

$$\begin{aligned} C_d &= \left(I + C(\alpha I - A)^{-1}L_T\right)C_{d_o} \\ D_d &= \left(I + C(\alpha I - A)^{-1}L_T\right)D_{d_o} \end{aligned} \tag{E.3}$$

By the operators defined earlier, it is possible to find:

$$\begin{aligned} y(k) - \hat{y}(k) = &\left(I - M_{d_o}\right)(C_d x(\zeta, k-1) + D_d u(k)) \\ &-C_{d_o}\hat{x}(\zeta, k-1) - D_{d_o}u(k) \end{aligned} \tag{E.4}$$

Then, from Eqs. (E.3) and (E.4), one can write:

$$\begin{aligned} &y(k) - \hat{y}(k) = (I - M_d)\left(I + C(\alpha I - A)^{-1}L_T\right)\left(C_{d_o}x(\zeta, k-1) + D_{d_o}u(k)\right) \\ &\quad -C_{d_o}\hat{x}(\zeta, k-1) - D_{d_o}u(k) \rightarrow \\ &I - M_{d_o} = I - \left(I + C(\alpha - A)^{-1}L_T\right)^{-1}C(\alpha I - A)^{-1}L_T \\ &= \left(I + C(\alpha I - A)^{-1}L_T\right)^{-1}\left(I + C(\alpha I - A)^{-1}L_T - C(\alpha I - A)^{-1}L_T\right) \\ &= \left(I + C(\alpha I - A)^{-1}L_T\right)^{-1} \rightarrow y(k) - \hat{y}(k) = -\left(C_{d_o}x(\zeta, k-1) + D_{d_o}u(k)\right) \\ &\quad +\left(I + C(\alpha I - A)^{-1}L_T\right)^{-1}\left(I + C(\alpha I - A)^{-1}L_T\right)\left(C_{d_o}x(\zeta, k-1) + D_{d_o}u(k)\right) \\ &= C_{d_o}\left(x(\zeta, k-1) - \hat{x}(\zeta, k-1)\right) \end{aligned} \tag{E.5}$$

Hence, the discrete observer error takes the following form:

$$\begin{aligned} \hat{e}_d(\zeta, k) &= x(\zeta, k) - \hat{x}(\zeta, k) \\ &= A_d\left(x(\zeta, k-1) - \hat{x}(\zeta, k-1)\right) - L_d\left(y(k) - \hat{y}(k)\right) \\ &= (A_d - L_d C_{d_o})\hat{e}_d(\zeta, k-1) \end{aligned} \tag{E.6}$$

The above equation can be linked to the continuous time setting as below:

$$\begin{aligned} (A_d - L_d C_{d_o}) &= -I + 2\alpha(\alpha - A)^{-1} \\ &\quad -2\alpha\left[I - \left(I + (\alpha I + A)^{-1}L_T C\right)^{-1}\right](\alpha I - A)^{-1} \\ &= -I + 2[\alpha I - A + L_T C]^{-1} = -I + 2[\alpha I - A_o]^{-1} \end{aligned} \tag{E.7}$$

which would be the discrete version of $A_o = A - L_T C$. Therefore, if the selected continuous observer gain L_T ensures that the operator A_o is stable, then the discrete version of the observer is stable as well.

References

Aksikas, I., Moghadam, A.A., Forbes, J.F., 2017. Optimal linear–quadratic control of coupled parabolic–hyperbolic PDEs. Int. J. Control 90 (10), 2152–2164. doi:10.1080/00207179.2016.1237046.

Alonso, A.A., Kevrekidis, I.G., Banga, J.R., Frouzakis, C.E., 2004. Optimal sensor location and reduced order observer design for distributed process systems. Comput. Chem. Eng. 28 (1), 27–35. doi:10.1016/S0098-1354(03)00175-3. Escape 12.

Antoniades, C., Christofides, P., 2000. Non-linear feedback control of parabolic partial differential difference equation systems. Int. J. Control 73 (17), 1572–1591. doi:10.1080/00207170050197696.

Antoniades, C., Christofides, P.D., 2001. Studies on nonlinear dynamics and control of a tubular reactor with recycle. Nonlinear Anal. 47 (9), 5933–5944. doi:10.1016/S0362-546X(01)00699-X.

Armaou, A., Christofides, P.D., 2002. Dynamic optimization of dissipative PDE systems using nonlinear order reduction. Chem. Eng. Sci. 57 (24), 5083–5114. doi:10.1016/S0009-2509(02)00419-0.

Aström, K.J., Wittenmark, B., 1990. Computer-Controlled Systems: Theory and Design, second ed. Prentice Hall, Engelwood Cliffs.

Badillo-Hernandez, U., Alvarez, J., Alvarez-Icaza, L., 2019. Efficient modeling of the nonlinear dynamics of tubular heterogeneous reactors. Comput. Chem. Eng. 123, 389–406. doi:10.1016/j.compchemeng.2019.01.018.
Balas, M.J., 1979. Feedback control of linear diffusion processes. Int. J. Control 29 (3), 523–534. doi:10.1080/00207177908922716.
Bildea, C.S., Dimian, A.C., Cruz, S.C., Iedema, P.D., 2004. Design of tubular reactors in recycle systems. Comput. Chem. Eng. 28 (1), 63–72. doi:10.1016/S0098-1354(03)00170-4. Escape 12.
Bitzer, M., Zeitz, M., 2002. Design of a nonlinear distributed parameter observer for a pressure swing adsorption plant. J. Process. Control 12 (4), 533–543. doi:10.1016/S0959-1524(01)00019-1.
Bizon, K., Continillo, G., Russo, L., Smua, J., 2008. On pod reduced models of tubular reactor with periodic regimes. Comput. Chem. Eng. 32 (6), 1305–1315. doi:10.1016/j.compchemeng.2007.06.004.
Bonis, I., Xie, W., Theodoropoulos, C., 2012. A linear model predictive control algorithm for nonlinear large-scale distributed parameter systems. AIChE J. 58 (3), 801–811. doi:10.1002/aic.12626.
Bokovi, D.M., Krsti, M., 2002. Backstepping control of chemical tubular reactors. Comput. Chem. Eng. 26 (7), 1077–1085. doi:10.1016/S0098-1354(02)00026-1.
Christofides, P.D., Daoutidis, P., 1997. Finite-dimensional control of parabolic PDE systems using approximate inertial manifolds. J. Math. Anal. Appl. 216 (2), 398–420. doi:10.1006/jmaa.1997.5649.
Cohen, D.S., Poore, A.B., 1974. Tubular chemical reactors: the “lumping approximation” and bifurcation of oscillatory states. SIAM J. Appl. Math. 27 (3), 416–429. doi:10.1137/0127032.
Curtain, R., 1982. Finite-dimensional compensator design for parabolic distributed systems with point sensors and boundary input. IEEE Trans. Autom. Control 27 (1), 98–104. doi:10.1109/TAC.1982.1102875.
Curtain, R.F., Zwart, H., 1995. An introduction to Infinite-Dimensional Linear Systems Theory. New York: Springer-Verlag doi:10.1137/1038096.
Danckwerts, P., 1953. Continuous flow systems: distribution of residence times. Chem. Eng. Sci. 2 (1), 1–13. doi:10.1016/0009-2509(53)80001-1.
Dochain, D., 2000. State observers for tubular reactors with unknown kinetics. J. Process. Control 10 (2), 259–268. doi:10.1016/S0959-1524(99)00020-7.
Dochain, D., 2001. State observation and adaptive linearizing control for distributed parameter (bio)chemical reactors. Int. J. Adapt. Control Signal Process. 15 (6). doi:10.1002/acs.691.
Dochain, D., 2018. Analysis of the multiplicity of steady-state profiles of two tubular reactor models. Comput. Chem. Eng. 114, 318–324. doi:10.1016/j.compchemeng.2017.10.028.
Dubljevic, S., El-Farra, N.H., Mhaskar, P., Christofides, P.D., 2006. Predictive control of parabolic PDEs with state and control constraints. Int. J. Robust Nonlinear Control 16 (16), 749–772. doi:10.1002/rnc.1097.
Dufour, P., Tour, Y., Blanc, D., Laurent, P., 2003. On nonlinear distributed parameter model predictive control strategy: on-line calculation time reduction and application to an experimental drying process. Comput. Chem. Eng. 27. doi:10.1016/S0098-1354(03)00099-1.
Franklin, G.F., Powell, J.D., Workman, M.L., et al., 1998. Digital Control of Dynamic Systems, 3. Addison-Wesley, Reading.
Georgakis, C., Aris, R., Amundson, N.R., 1977. Studies in the control of tubular reactors-i general considerations. Chem. Eng. Sci. 32 (11), 1359–1369. doi:10.1016/0009-2509(77)85032-X.
Hairer, E., Lubich, C., Wanner, G., 2006. Geometric Numerical Integration: Structure-Preserving Algorithms for Ordinary Differential Equations, 31. Springer Science & Business Media.
Hastir, A., Lamoline, F., Winkin, J.J., Dochain, D., 2020. Analysis of the existence of equilibrium profiles in nonisothermal axial dispersion tubular reactors. IEEE Trans. Autom. Control 65 (4), 1525–1536. doi:10.1109/TAC.2019.2921675.
Heinemann, R.F., Poore, A.B., 1982. The effect of activation energy on tubular reactor multiplicity. Chem. Eng. Sci. 37 (1), 128–131. doi:10.1016/0009-2509(82)80079-1.
Hlavacek, V., Hofmann, H., 1970. Modeling of chemical reactors - xvi: steady state axial heat and mass transfer in tubular reactors - an analysis of the uniqueness of solutions. Chem. Eng. Sci. 25 (1), 187–199. doi:10.1016/0009-2509(70)85031-X.
Hlavacek, V., Hofmann, H., 1970. Modeling of chemical reactors - xvii: steady state axial heat and mass transfer in tubular reactors - numerical investigation of multiplicity. Chem. Eng. Sci. 25 (1), 173–185. doi:10.1016/0009-2509(70)85030-8.
Jensen, K.F., Ray, W., 1982. The bifurcation behavior of tubular reactors. Chem. Eng. Sci. 37 (2), 199–222. doi:10.1016/0009-2509(82)80155-3.
Kazantzis, N., Kravaris, C., 1999. Energy-predictive control: a new synthesis approach for nonlinear process control. Chem. Eng. Sci. 54 (11), 1697–1709. doi:10.1016/S0009-2509(98)00499-0.
Levenspiel, O., 1999. Chemical reaction engineering. Ind. Eng. Chem. Res. 38 (11), 4140–4143. doi:10.1021/ie990488g.
Liu, Y., Jacobsen, E.W., 2004. On the use of reduced order models in bifurcation analysis of distributed parameter systems. Comput. Chem. Eng. 28 (1), 161–169. doi:10.1016/S0098-1354(03)00183-2.
Luss, D., Amundson, N.R., 1967. Stability of loop reactors. AIChE J. 13 (2), 279–290. doi:10.1002/aic.690130218.
Marwaha, B., Luss, D., 2003. Hot zones formation in packed bed reactors. Chem. Eng. Sci. 58 (3), 733–738. doi:10.1016/S0009-2509(02)00602-4.
Mayne, D.Q., 2014. Model predictive control: recent developments and future promise. Automatica 50 (12), 2967–2986. doi:10.1016/j.automatica.2014.10.128.
Mohd Ali, J., Ha Hoang, N., Hussain, M., Dochain, D., 2015. Review and classification of recent observers applied in chemical process systems. Comput. Chem. Eng. 76, 27–41. doi:10.1016/j.compchemeng.2015.01.019.
Muske, K.R., Rawlings, J.B., 1993. Model predictive control with linear models. AIChE J. 39 (2), 262–287. doi:10.1002/aic.690390208.
Rawlings, J., Mayne, D., Diehl, M., 2017. Model Predictive Control: Theory, Computation, and Design. Nob Hill Publishing, LLC, Madison.
Ray, W., 1981. Advanced Process Control.. McGraw Hill, New York.
Varma, A., Aris, R., 1977. Stirred pots and empty tubes. In: Chemical Reactor Theory. Prentice-Hall, pp. 79–154.
V.Havu, Malinen, J., 2007. The Cayley transform as a time discretization scheme. Numerical Funct. Anal. Optim. 28 (7–8), 825–851. doi:10.1080/01630560701493321.
Xie, J., Xu, Q., Ni, D., Dubljevic, S., 2019. Observer and filter design for linear transport-reaction systems. Eur. J. Control 49, 26–43. doi:10.1016/j.ejcon.2019.01.005.
Xu, Q., Dubljevic, S., 2017. Linear model predictive control for transport-reaction processes. AIChE J. 63 (7), 2644–2659. doi:10.1002/aic.15592.
Xu, X., Dubljevic, S., 2016. Output regulation problem for a class of regular hyperbolic systems. Int. J. Control 89 (1), 113–127. doi:10.1080/00207179.2015.1060363.